International Geology Review
iFirst article, 2009, 1–31

Geochemical evidence of a near-surface history for source rocks of the central Coast Mountains Batholith, British Columbia

Paul H. Wetmore[a] and Mihai N. Ducea[b]*

[a]*Department of Geology, University of South Florida, Tampa, FL 33620, USA;* [b]*Department of Geosciences, University of Arizona, Tucson, AZ 85721, USA*

(*Accepted 3 May 2009*)

Major and trace elemental concentrations as well as Sr and Pb isotopic data, obtained for 41 plutonic samples from the Coast Mountains Batholith ranging in age from ~108 to ~50 Ma, indicate that the source regions for these rocks were relatively uniform and typical of Cordilleran arcs. The studied rocks are mineralogically and chemically metaluminous to weakly peraluminous and are mainly calc-alkaline. Initial whole-rock $^{87}Sr/^{86}Sr$ ratios range from 0.7035 up to 0.7053, whereas lead isotopic data range from 18.586 to 19.078 for $^{206}Pb/^{204}Pb$, 15.545 to 15.634 for $^{207}Pb/^{204}Pb$, and 37.115 to 38.661 for $^{208}Pb/^{204}Pb$. In contrast to these relatively primitive isotopic data, $\delta^{18}O$ values for quartz separates determined for 19 of the samples range from 6.8 up to 10.0‰. These $\delta^{18}O$ values preclude the possibility that these melts were exclusively generated from the Mesozoic mantle wedge of this continental arc, just as the Sr and Pb data preclude significant involvement of an old (Precambrian) crustal/mantle lithospheric source. We interpret the high $\delta^{18}O$ component to represent materials that had a multi-stage crustal evolution. They were originally mafic rocks derived from a circum-Pacific juvenile mantle wedge that experienced a period of near-surface residence after initial crystallization. During this interval, these primitive rocks interacted with meteoric waters at low temperatures, as indicated by the high $\delta^{18}O$ values. Subsequently, these materials were buried to lower crustal depths where they remelted to form the high $\delta^{18}O$ component of the Coast Mountains Batholith. This component makes up at least 40% (mass) of the Cretaceous through Eocene batholith in the studied area. The remainder of the source materials comprising the Coast Mountains Batholith had to be new additions from the mantle wedge. A prolonged period of contractional deformation beginning with the Early Cretaceous collisional accretion of the Insular superterrane is inferred to have been responsible for underthrusting the high $\delta^{18}O$ component into the lower crust. We suggest that mafic rocks of the Insular superterrane (e.g. Alexander–Wrangellia) are of appropriate composition, and were accreted to and overthrust by what would become the Coast Mountains Batholith just prior to initiation of magmatism in the region.

Keywords: Insular superterrane; lithospheric column; Coast Mountains Batholith

Introduction

Primary subduction-related basaltic magmas form by a combination of adiabatic and water flux melting in the mantle wedge above the downgoing slab (Gill 1981; Arculus 1994; Grove *et al.* 2003). Mantle-derived melts are modified in the upper plate via remelting, fractionation, assimilation, and mixing with upper plate melts (Petford and Atherton 1996; Dufek and Bergantz 2005; Annen *et al.* 2006). Petrologic, geochemical, and isotopic

*Corresponding author. Email: ducea@email.arizona.edu

ISSN 0020-6814 print/ISSN 1938-2839 online

DOI: 10.1080/00206810903028219
http://www.informaworld.com

variations of arc magmas, particularly those measured transverse to the arc trends (e.g. Kistler and Peterman 1978), are commonly ascribed to changes in the age, composition, and relative abundance of deep crustal or upper-mantle source rocks (DePaolo 1981; Kistler 1990; Chen and Tilton 1991; DeCelles *et al.* 2009).

In this study, we present new major and trace element as well as strontium, lead, and oxygen isotopic data from two transects across the Coast Mountains Batholith of west-central British Columbia, Canada. These geochemical data were acquired in conjunction with companion U–Pb geochronologic (Gehrels *et al.* in press) and Nd isotopic (Girardi *et al.* 2009) studies with the goal of constraining the compositional evolution of the arc lithospheric column, including source regions, of the Coast Mountains Batholith through time. We use elemental and isotopic data to argue that in addition to mantle-derived magmas, the arc had significant input from a high $\delta^{18}O$ component, which we interpret to represent tectonically underplated mafic crust of the Insular superterrane. This interpretation underscores the significance of subduction erosion/tectonic underplating processes in continental subduction systems and their role in arc magmatism.

Background geology

The Coast Mountains Batholith of west-central British Columbia comprises large, elongate coast-parallel intrusive belts (Barker *et al.* 1986; Figure 1). These intrusives can be divided into five groups based on geography and age of intrusives similar to the designations of van der Hayden (1992). From west to east, these intrusive belts include the

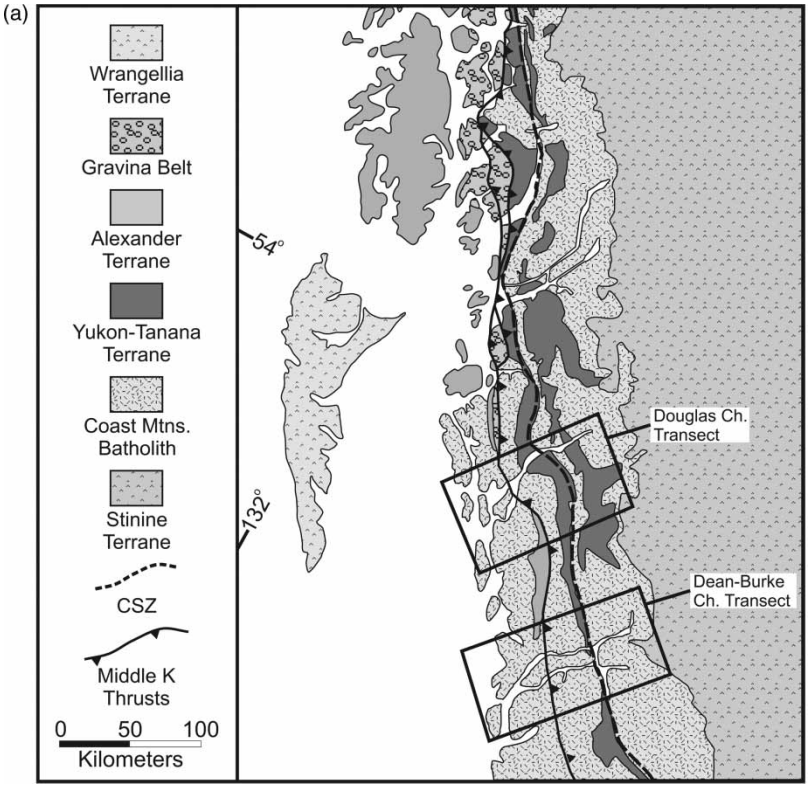

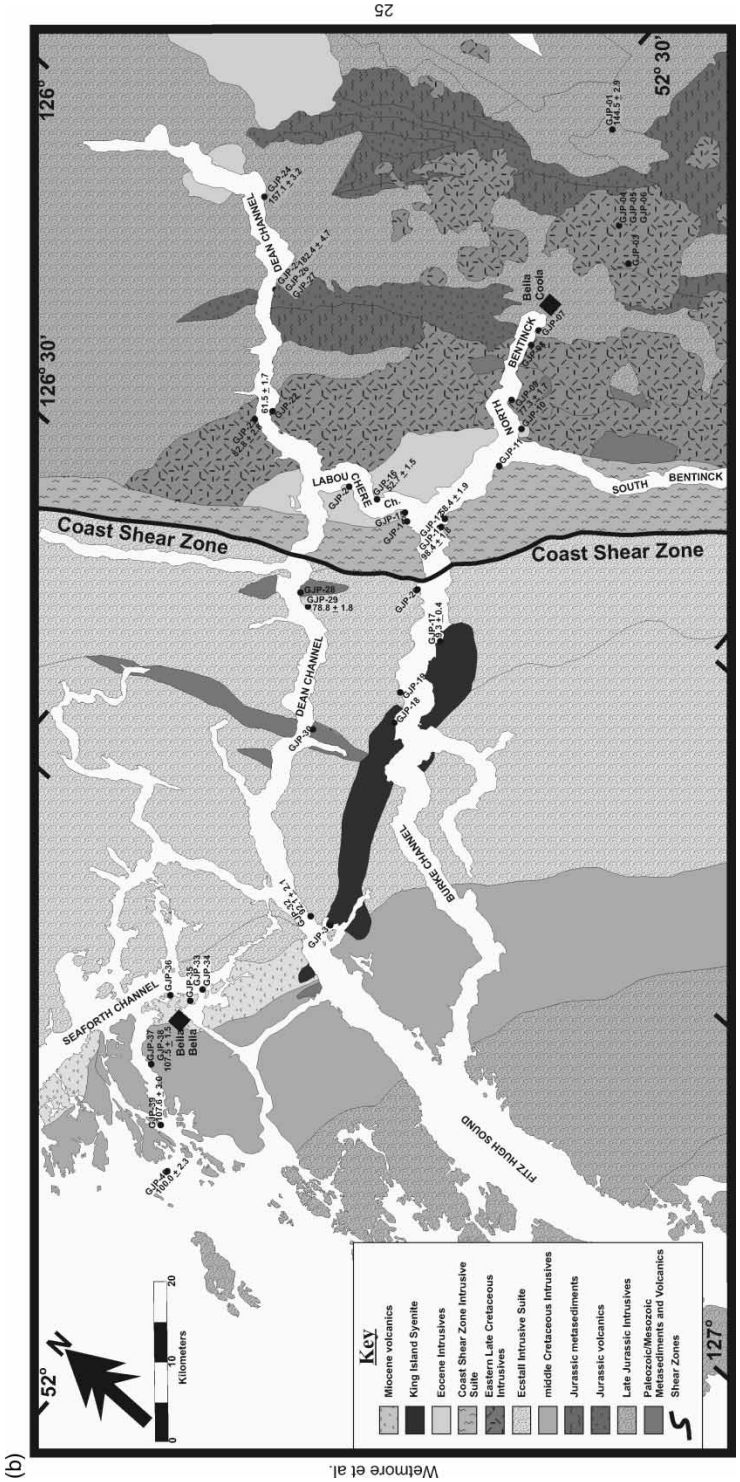

(b)

Wetmore et al.

25

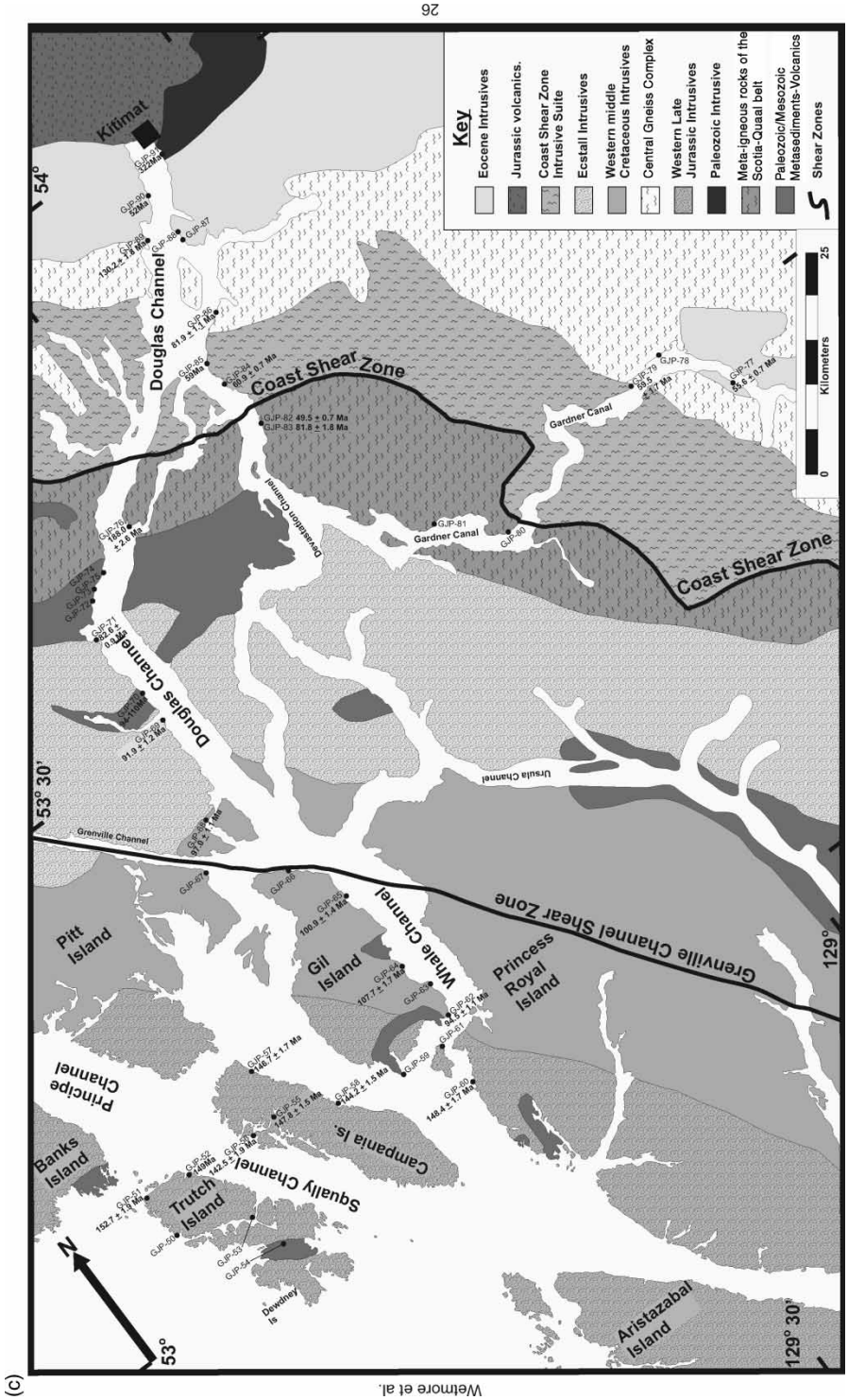

Figure 1. (a) Simplified regional geologic maps showing locations of both transects from this study. (b) The Dean–Burke Channel transect and (c) the Douglas Channel transect. The maps are modified from Wheeler and McFeely (1991) using more detailed mapping from Gareau and Woodsworth (2000), Rusmore *et al.* (2001), Haggart *et al.* (2004), and unpublished field mapping by Gehrels, G. (written communication, 2004). Ages shown adjacent to some sample localities are in millions of years and are from Gehrels *et al.* (in press).

western middle Cretaceous intrusives, the Ecstall-equivalent intrusives, the Coast Shear Zone (CSZ) intrusives, latest Palaeocene–Eocene intrusives, and the eastern Late Cretaceous intrusives. Also present within the map area are both western and eastern Late Jurassic and Miocene intrusives. Data from these intrusive suites are not included in this study due to their controversial and potentially unrelated tectonic setting.

The Coast Mountains Batholith straddles the boundary between the Insular and Intermontane superterranes (Monger *et al.* 1982). The CSZ is one of several northeast dipping, southwest vergent ductile shear zones that accommodated coast-normal contraction during the middle and Late Cretaceous through Palaeocene (Gehrels and Saleeby 1987; McClelland *et al.* 1992; Klepeis *et al.* 1998; Crawford *et al.* 2000; Rusmore *et al.* 2000). Contemporaneous with Coast Mountains arc magmatism, the rocks within and surrounding the study area experienced dextral transpression during the Late Cretaceous (Andronicos *et al.* 1999; Hollister and Andronicos 2006), and massive extension and exhumation during the latest Late Cretaceous through early Eocene.

Plutonic rocks sampled for this study are intermediate in composition, ranging from tonalites to granites. These rocks are, however, very homogeneous at the outcrop scale. The CSZ intrusives represent a major exception to this generalization as more than half of all exposures exhibit strong subsolidus fabrics with alternating mafic and leucocratic selvages (e.g. Ingram and Hutton 1994). For this study, these intrusives were sampled in areas least affected by shearing (Andronicos *et al.* 2003; Rusmore *et al.* 2005).

Analytical methods

Major and trace elements

The concentrations of major elements were determined at Macalester College using a Philips PW-2400 X-ray fluorescence spectrometer with Rh-anode, end-window X-ray tube, and Philips Super-Q analytical software. Sample preparation and analytical techniques conform to those described by Vervoort *et al.* (2007).

Trace element concentration analyses were conducted at the Department of Geological Sciences, University of Saskatchewan, Canada, by means of inductively coupled plasma mass spectrometry (ICP-MS). Powdered rock samples were prepared by the $HF–HNO_3$ digestion procedure, where approximately 100 mg of sample was dissolved in a ≈ 10 ml mixture consisting of equal amounts of double-distilled HF (48–51%) and of 16 N HNO_3 placed on a hot plate at 100–150°C for 3–6 days. Solutions were evaporated and the samples were redissolved in ~ 2.5 ml of 8 N HNO_3 and diluted by adding ~ 100 ml of Milli-Q water. Samples were analysed on a SCIEX ELAN model 250 ICP-MS following the techniques of Jenner *et al.* (1990) and Longerich *et al.* (1990).

Radiogenic isotopes

All sample preparation and analysis for radiogenic isotopes were conducted at the University of Arizona. Uncrushed, whole-rock samples used in this study were inspected and cleaned to ensure that no portion of any sample contained pieces that came in contact with the metal hammer during sample collection. Each sample was then powdered using an alumina shatter box. Between 100 and 400 mg of sample powders were weighed, put in Teflon beakers, and dissolved in mixtures of hot, concentrated $HF–HNO_3$. High purity $12\,mol\,l^{-1}$ HCl, $16\,mol\,l^{-1}$ HNO_3, and $28\,mol\,l^{-1}$ HF acids from Seastar Chemicals, Sydney, Canada, were used for all dissolutions and elemental isolations. Dilute solutions of high purity acids were prepared with purified water (18 mΩ) from a Millipore system.

Elemental isolation was performed in a crown-ether-based Sr-Spec resin, with a particle size between 100 and 150 μm (available commercially from Eichrom Technologies, Darlen, IL, USA). Column loads were between 0.25 and 0.5 ml. The method involves passage of 1 ml of sample solution in 3.5 mol l^{-1} HNO_3 medium through the extraction column, which retains strontium. Rubidium and other matrix elements are washed from the column leaving a pure strontium fraction on column. The strontium is then stripped with a small volume of diluted nitric acid (0.05 mol l^{-1} HNO_3). Following strontium extraction, the column is treated with 2 N HCl and lead is then extracted with 8 N HCl. Following isolation of strontium and lead, each sample was evaporated and redissolved in dilute ($\sim$1%) HNO_3.

Strontium analyses were conducted on a Micromass Isoprobe, a multicollector inductively coupled plasma mass spectrometer (MC-ICP-MS) following the procedures described in detail by Ducea *et al.* (2009). Samples were analysed in solution with measurements made in static mode where collectors were fixed to track masses 85, 86, 87, and 88, simultaneously for strontium.

Washes from the cation column separation were used for separating Pb in Sr-Spec resin (Eichrom, Darien, IL, USA) columns by using a protocol developed at the University of Arizona. Samples were loaded in 8 M HNO_3 in the Sr-spec columns. Pb elution was achieved via 8 M HCl. Lead isotope analysis was conducted on a GV Instruments (Hudson, NH, USA) MC-ICP-MS at the University of Arizona (Thibodeau *et al.* 2007). Samples were introduced into the instrument by free aspiration with a low-flow concentric nebulizer into a water-cooled chamber. A blank, consisting of 2% HNO_3, was run before each sample. Before analysis, all samples were spiked with a Tl solution to achieve a Pb/Tl ratio of $\approx$ 10. Throughout the experiment, the standard National Bureau of Standards (NBS)-981 was run to monitor the stability of the instrument.

All results were Hg-corrected and empirically normalized to Tl by using an exponential law correction. To correct for machine and interlaboratory bias, all results were normalized to values reported by Galer and Abouchami (2004) for the National Bureau of Standards (NBS)-981 standard ($^{206}Pb/^{204}Pb = 16.9405$, $^{207}Pb/^{204}Pb = 15.4963$, and $^{208}Pb/^{204}Pb = 36.7219$). The internal error reflects the reproducibility of the measurements on individual samples, whereas external errors are derived from long-term reproducibility of NBS-981 Pb standard and result in part from the mass bias effects within the instrument. In all cases, external error exceeds the internal errors and is reported below. External errors associated with each Pb isotopic ratio are as follows: $^{206}Pb/^{204}Pb = 0.028\%$, $^{207}Pb/^{204}Pb = 0.028\%$, and $^{208}Pb/^{204}Pb = 0.031\%$.

Oxygen isotopes

Oxygen isotopic data were collected at the University of Arizona with some duplicate analyses completed on select samples in the stable isotope laboratory of the Department of Earth and Planetary Sciences at the University of New Mexico. The data were generated from quartz separates hand-picked from samples exhibiting negligible alteration of feldspars, as determined through petrographic inspection. Quartz $\delta\ ^{18}O$ values were generated by conventional techniques employing bromine pentafluoride (BrF_5) as the fluorinating agent. Three to eight milligrams of each sample were heated to $\sim$650°C in sealed nickel vessels for 6–10 h in the presence of excess BrF_5 to generate O_2. The O_2 was next reacted with hot platinized graphite to produce CO_2. Calculated yields were typically 100 $\pm$ 5%. The isotopic composition of CO_2 was then measured on a Finnigan MAT Delta S mass spectrometer. Samples were calibrated against in-house and public standards

including GJP-16 which was analysed multiple times and processed in alternating decomposition vessels to ensure consistent results for each part of the system. Analyses of all samples were repeated two or three times on separate fractions of the same quartz separates. The precision of the results was better than $\pm 0.2‰$.

Petrology and geochemistry

Petrology

The rocks from west of the CSZ are, in order of abundance, mostly granodiorites and tonalites, are granular and coarse grained, and primarily consist of quartz, alkali, and plagioclase feldspar. The most abundant mafic minerals are both Mg- and Fe-rich hornblendes and biotite with accessory minerals that include apatite, epidote, titanite, and zircon. In addition, Fe–Ti oxides are quite common in most of the samples, especially in those comprising the western middle Cretaceous intrusives. Nearly all samples exhibit limited amounts of late magmatic to high-temperature subsolidus deformation as exemplified by undulatory extinction in quartz and minor sub-grain development along quartz–quartz crystal boundaries.

The average modal abundance of quartz within the intrusive groups west of the CSZ is 33% for the Ecstall and 30% for the western middle Cretaceous. The crystals are usually anhedral to subhedral (rounded or sub-rounded) with patchy and/or undulatory extinction. Alkali feldspars (22 and 20%) form enclaves or clusters of large phenocrysts and are dominantly orthoclase and microcline. Plagioclase (29 and 32%) is relatively fresh, with a compositional range between An_{14} and An_{34} or from oligoclase to andesine. Almost all the crystals show polysynthetic twinning and oscillatory zoning. Hornblende (8 and 6%) is the dominant mafic mineral, identified in every sample from west of the CSZ. Biotite (6 and 9%) crystals are tabular, subhedral to anhedral.

Samples of the Ecstall-equivalent intrusives, which include those from the southern end of the Ecstall pluton (Hutchison 1982; Zen and Hammarstrom 1984; Butler *et al.* 2002), are characterized by the presence of primary epidote. Epidote has a modal abundance of 2% or less in all of the Ecstall-equivalent samples with crystal lengths less than 0.6 cm.

As with samples from the west, those from east of the CSZ exhibit similar compositions; granodiorites and tonalities in addition to which there are several granites. They are mostly coarse grained exhibiting porphyritic and seldom granitic textures. The modal compositions of the eastern suite of samples are broadly similar to those from the west with the most salient differences being greater modal abundances of quartz and alkali feldspars at the expense of hornblende.

The average modal abundance of quartz in all samples from east of the CSZ is 34% for the Eocene, 32% for the CSZ intrusive, and 35% for the Early Cretaceous. Most crystals are anhedral, and are intergranular between larger feldspar crystals. Subsolidus deformation (i.e. undulatory extinction and subgrain development) is observable in nearly all samples, but is most strongly developed within samples from CSZ intrusives. Alkali feldspars (23, 25, and 26%), which include microcline and orthoclase, are subhedral to anhedral in all eastern intrusive suites. Some subhedral orthoclase crystals show poikilitic texture in which small quartz, biotite, and opaques represent chadacryst assemblages. Plagioclase feldspar (33, 34, and 31%) is characterized by compositions that range from An_3 to An_{29}. Biotite (7, 6, and 8%) is the most common mafic mineral present in all samples from east of the CSZ. Biotite occurs as subhedral crystals of considerable length (up to 1.2 cm). Hornblende, which is restricted to samples from the eastern Late Cretaceous intrusives, is anhedral and has a modal abundance less than 1%.

In some samples from the Eocene intrusives, trace amounts of small (<1 mm) pyroxene (aegirine–augite) phenocrysts are observed, which are entirely shattered and partially transformed by subsolidus alteration into epidote, chlorite and opaque, Fe-rich oxides. Trace amounts of garnet were also observed in one sample from eastern Late Cretaceous intrusives.

Elemental chemistry

The major elemental compositions of all groups of intrusives are presented in Tables 1(a) (western) and 2(a) (eastern) and plotted in Harker diagrams in Figure 2. Additionally, alumina saturation is illustrated for all samples in the A/NK–A/CNK plot of Figure 3. With rare exception, all samples analysed in this study are calc-alkaline and most are metaluminous to weakly peraluminous. Collectively, all samples define typical elemental trends on Harker diagrams with TiO_2, Al_2O_3, MgO, CaO, P_2O_5, FeO_t (total Fe), and MnO decreasing and K_2O increasing with increasing silica. However, while most samples define increasing concentrations of Na_2O with increasing silica, the Ecstall intrusives define a scattered but decreasing trend.

Trace elemental data are provided in Tables 1(b),(c) (western) and 2(b),(c) (eastern). Incompatible-element plots normalized to mid-ocean ridge basalts (MORBs; Pearce 1983) for all groups of intrusives are shown in Figure 4. They illustrate relatively minor depletions of Ti and heavy rare-earth elements (HREEs), and enrichments in various large-ion lithophile elements such as Ba, Th, and Rb, as well as LREEs. Light REE enrichment and HREE depletions are common to most samples from both transects on both sides of the CSZ, and do not exhibit a clear correlation with Eu anomalies (Figure 5).

Isotope geochemistry

Lead and strontium as well as oxygen isotopic ratios of whole-rock samples and quartz separates, respectively, collected from the central Coast Mountains Batholith are given in Table 3. Measured $^{87}Sr/^{86}Sr$ ratios were age-corrected using U/Pb zircon crystallization ages determined on the same samples collected for geochemistry (Gehrels *et al.* in press) and the elemental concentrations of Rb and Sr to calculate initial ratios. Initial $^{87}Sr/^{86}Sr$ ratios were determined for all 41 plutonic samples investigated in this study, and those ratios range from 0.7035 to 0.7053, with an average of 0.7042.

Measured $^{206}Pb/^{204}Pb$, $^{207}Pb/^{204}Pb$, and $^{208}Pb/^{204}Pb$ ratios were age-corrected using available U/Pb zircon crystallization ages and the elemental concentrations of Pb, Th, and U to calculate initial common lead ratios. Initial $^{206}Pb/^{204}Pb$, $^{207}Pb/^{204}Pb$, and $^{208}Pb/^{204}Pb$ ratios were determined for 40 out of the 41 plutonic samples investigated in this study and those ratios range from 18.586 to 19.078 with an average of 18.825 for $^{206}Pb/^{204}Pb_i$, from 15.545 to 15.634 with an average of 15.582 for $^{207}Pb/^{204}Pb_i$, and from 37.115 to 38.661 with an average of 38.287 for $^{208}Pb/^{204}Pb_i$.

Oxygen data were determined on 26 quartz separates of the 41 plutonic samples investigated in this study and from each of the Mesozoic and Tertiary belts of magmatism comprising the Coast Mountains Batholith. $\delta^{18}O$ values for the Coast Mountains Batholith samples range from 6.8 to 10.0‰ with an average of 8.4‰.

Compositional trends and variations

Geochemical variations

The petrography and major and trace elemental chemistry of all intrusive suites analysed in this study suggest that the source melts and compositional diversification trends that

Table 1(a). Major elements (wt%) composition for samples on the western side of the Coastal Shear Zone.

Sample	Intrusive group	Petrology	Age (Ma)	SiO_2	TiO_2	Al_2O_3	$Fe_2O_3^*$	MnO	MgO	CaO	Na_2O	K_2O	P_2O_5	LOI	FeOt	Total	A/CNK
GJP-19	EI	Granodiorite	*92.1 ± 2.1*	58.62	0.86	18.42	5.53	0.08	2.17	5.71	5.45	1.75	0.30	0.45	4.98	99.36	0.87
GJP-29	EI	Tonalite	78.8 ± 1.8	54.49	1.36	20.07	7.41	0.10	2.86	7.14	5.93	0.84	0.47	0.45	6.67	101.12	0.85
GJP-32	EI	Granite	92.1 ± 2.1	71.42	0.47	14.42	3.21	0.07	1.25	3.25	3.82	2.63	0.12	0.61	2.89	101.27	0.96
GJP-36	EI	Granodiorite	92.0 ± 2.5	64.03	0.62	17.93	3.79	0.07	1.36	4.68	5.31	1.95	0.19	0.35	3.41	100.27	0.93
GJP-44	EI	Granite	81.7 ± 0.9	67.86	0.50	16.20	3.26	0.06	1.20	3.20	4.69	2.85	0.16	0.38	2.93	100.36	0.97
GJP-69	EI	Granodiorite	91.9 ± 1.2	59.73	0.68	18.17	5.49	0.10	2.87	6.14	4.65	1.38	0.29	0.48	4.94	99.98	0.89
GJP-71	EI	Granodiorite	82.6 ± 0.9	64.08	0.67	16.79	4.65	0.07	2.13	4.83	4.15	2.03	0.18	0.4	4.18	99.98	0.94
GJP-83	EI	Granodiorite	81.8 ± 1.8	65.77	0.49	16.69	4.11	0.07	1.75	4.70	4.01	1.50	0.17	0.40	3.70	99.66	1
GJP-37	WMK	Granodiorite	107.5 ± 1.5	59.69	0.68	19.76	5.68	0.11	2.25	6.39	4.37	1.56	0.26	0.48	5.11	101.24	0.96
GJP-38	WMK	Tonalite	*107.5 ± 1.5*	49.75	1.08	20.13	10.65	0.19	4.28	8.89	4.11	1.16	0.37	0.62	9.58	101.22	0.83
GJP-39	WMK	Granite	107.6 ± 3.0	70.89	0.46	14.47	3.22	0.07	1.20	3.27	3.88	2.63	0.12	0.61	2.90	100.81	0.95
GJP-40	WMK	Granodiorite	100.0 ± 2.3	64.95	0.38	16.72	5.18	0.15	1.81	5.41	3.53	1.56	0.16	0.57	4.66	100.43	0.97
GJP-43	WMK	Tonalite	123.3 ± 1.4	50.99	1.14	19.15	9.74	0.17	5.01	9.34	3.76	0.34	0.29	0.39	8.76	100.30	0.81
GJP-62	WMK	Tonalite	94 ± 1.1	58.76	0.72	18.00	7.02	0.14	3.04	6.81	4.09	1.09	0.23	0.60	6.32	100.49	0.89
GJP-63	WMK	Granodiorite	*94 ± 1.1*	56.05	1.04	17.95	8.23	0.16	3.59	7.65	3.77	1.33	0.28	0.26	7.41	100.30	0.83
GJP-64	WMK	Granite	107.7 ± 1.7	70.39	0.27	15.23	2.81	0.14	0.73	3.10	3.98	2.36	0.12	0.55	2.53	99.68	1.03
GJP-65	WMK	Tonalite	100.9 ± 1.4	53.50	0.92	18.03	9.59	0.18	4.57	8.58	3.15	0.95	0.21	0.42	8.63	100.12	0.83
GJP-67	WMK	Tonalite	*97.0 ± 1.1*	53.18	1.06	18.89	9.30	0.18	4.12	8.15	3.77	1.12	0.36	0.55	8.37	100.69	0.85
GJP-68	WMK	Granodiorite	97.0 ± 1.1	59.33	0.92	16.58	6.71	0.12	3.62	5.99	3.90	2.32	0.30	0.58	6.04	100.38	0.84

Notes: EI, Ecstall intrusives; WMK, western middle Cretaceous intrusives. Ages are U/Pb zircon ages from Gehrels *et al.* (in press). Samples with italicized ages are extrapolated from adjacent dated samples of the same intrusive body or suite as determined by observed field relationships.

Table 1(b). Trace elements (ppm) composition for samples on the western side of the Coastal Shear Zone.

Sample	Intrusive group	Petrology	Ba	Rb	Sr	Zr	Nb	Ni	Co	Zn	Cr	Th	Ce	Pr	Nd	Sm
GJP-19	EI	Granodiorite	791.87	45.79	1539.76	102.93	14.91	6.76	13.86	142.88	15.61	4.84	92.24	11.60	43.97	7.79
GJP-29	EI	Tonalite	892.57	60.01	1151.90	97.52	6.24	12.93	16.49	125.09	37.18	4.38	48.06	6.34	25.93	5.09
GJP-32	EI	Granite	904.59	42.11	420.75	103.14	8.57	37.78	6.47	91.27	13.93	11.82	68.82	6.41	19.77	2.94
GJP-36	EI	Granodiorite	986.23	37.45	827.13	90.79	6.81	4.00	9.71	125.76	17.58	3.47	39.85	4.50	16.23	2.68
GJP-44	EI	Granite	1220.87	65.58	669.69	179.04	11.76	4.90	7.72	85.13	13.92	6.09	53.40	6.07	21.36	3.76
GJP-69	EI	Granodiorite	771.19	32.68	982.12	111.31	7.94	22.26	18.07	81.37	59.84	1.34	30.52	4.02	16.41	3.45
GJP-71	EI	Granodiorite	999.72	50.22	650.77	111.88	5.82	7.48	13.74	74.38	29.56	4.13	26.88	3.72	15.74	3.68
GJP-83	EI	Granodiorite	671.87	38.81	586.54	62.28	4.31	8.55	10.51	68.42	26.92	3.79	38.01	4.52	16.65	2.83
GJP-37	WMK	Granodiorite	675.47	38.12	747.63	271.36	12.18	3.56	14.21	100.30	17.94	7.20	58.59	6.96	26.35	5.27
GJP-38	WMK	Tonalite	553.99	27.67	863.16	129.65	8.24	6.07	29.82	166.61	37.46	1.37	41.60	5.48	23.25	5.28
GJP-39	WMK	Granite	905.84	42.76	416.10	106.13	11.66	4.24	7.23	118.21	17.71	7.95	64.79	6.74	22.57	3.89
GJP-40	WMK	Granodiorite	608.29	34.63	569.74	69.91	5.94	3.15	9.96	142.44	17.02	1.91	21.70	2.92	11.88	2.68
GJP-43	WMK	Tonalite	279.33	3.63	739.16	45.73	7.05	14.95	37.72	107.43	49.37	0.16	25.48	3.43	14.79	3.55
GJP-62	WMK	Tonalite	424.97	21.92	650.66	151.49	8.90	9.68	19.87	76.43	35.87	3.18	29.32	3.48	12.79	2.76
GJP-63	WMK	Granodiorite	628.59	31.19	591.52	137.21	10.76	5.14	27.58	87.24	24.09	2.69	39.83	5.30	21.26	5.18
GJP-64	WMK	Granite	918.67	64.68	445.64	154.44	18.99	1.97	5.47	61.87	10.74	6.06	54.34	6.28	21.78	4.09
GJP-65	WMK	Tonalite	437.38	21.26	662.12	149.72	7.29	92.43	35.49	81.16	37.18	1.70	27.34	3.74	15.50	3.66
GJP-67	WMK	Tonalite	553.19	16.72	623.41	72.56	8.12	5.56	29.52	80.58	32.57	0.93	32.24	4.33	18.35	4.22
GJP-68	WMK	Granodiorite	1239.63	54.74	800.26	169.84	12.75	11.22	18.04	86.84	61.39	5.21	56.29	7.24	27.91	5.57

Notes: EI, Ecstall intrusives; WMK, western middle Cretaceous intrusives.

Table 1(c). Trace elements (ppm) composition for samples on the western side of the Coastal Shear Zone.

Sample	Intrusive group	Petrology	Eu	Gd	Tb	Dy	Ho	Er	Tm	Yb	Lu	Y	Cs	Ta	Hf	U	La/Yb	Eu/Eu*
GJP-19	EI	Granodiorite	2.09	6.03	0.67	3.42	0.58	1.50	0.20	1.23	0.16	16.62	0.77	1.11	3.14	0.91	31.1	0.9
GJP-29	EI	Tonalite	1.45	4.19	0.52	2.84	0.52	1.46	0.20	1.28	0.18	14.88	1.18	0.47	3.01	1.93	16.7	0.9
GJP-32	EI	Granite	0.86	2.54	0.29	1.65	0.31	0.91	0.13	0.89	0.13	9.10	0.63	0.77	3.12	2.16	49.6	0.9
GJP-36	EI	Granodiorite	0.92	2.02	0.23	1.27	0.23	0.63	0.09	0.64	0.08	7.49	1.47	0.49	2.84	1.45	29.9	1.2
GJP-44	EI	Granite	1.06	3.08	0.35	1.87	0.31	0.89	0.11	0.76	0.10	10.80	0.98	0.79	4.40	1.72	35.5	0.9
GJP-69	EI	Granodiorite	1.13	3.03	0.39	2.22	0.41	1.13	0.15	0.96	0.13	12.31	0.82	0.37	2.82	0.99	14.3	1.0
GJP-71	EI	Granodiorite	1.07	3.43	0.45	2.45	0.43	1.11	0.15	0.92	0.13	12.66	0.68	0.35	3.17	1.83	12.9	0.9
GJP-83	EI	Granodiorite	0.88	2.34	0.26	1.34	0.23	0.58	0.08	0.54	0.07	7.47	0.82	0.22	1.77	0.42	34.8	1.0
GJP-37	WMK	Granodiorite	1.84	4.93	0.68	4.28	0.84	2.54	0.36	2.47	0.35	23.00	0.86	1.17	6.65	1.29	12.1	1.1
GJP-38	WMK	Tonalite	1.77	5.45	0.78	4.78	0.97	2.86	0.41	2.69	0.39	25.63	0.43	0.40	3.28	0.48	6.8	1.0
GJP-39	WMK	Granite	1.08	3.26	0.39	2.27	0.43	1.27	0.18	1.22	0.17	12.40	0.54	1.06	3.26	2.20	29.7	0.9
GJP-40	WMK	Granodiorite	0.90	2.67	0.39	2.51	0.53	1.57	0.25	1.83	0.27	14.45	1.37	0.56	2.20	1.02	5.2	1.0
GJP-43	WMK	Tonalite	1.29	3.74	0.54	3.40	0.67	1.92	0.28	1.84	0.25	19.06	0.20	0.34	1.22	0.09	6.1	1.1
GJP-62	WMK	Tonalite	1.00	2.91	0.41	2.62	0.52	1.54	0.22	1.52	0.23	15.21	0.95	0.69	3.77	1.26	9.6	1.1
GJP-63	WMK	Granodiorite	1.37	5.55	0.85	5.30	1.08	3.20	0.46	2.98	0.44	30.03	1.14	0.59	3.58	1.08	5.8	0.8
GJP-64	WMK	Granite	1.12	4.01	0.59	3.73	0.79	2.48	0.39	2.82	0.44	23.30	1.21	1.39	4.45	3.32	9.6	0.8
GJP-65	WMK	Tonalite	1.22	3.98	0.62	3.69	0.76	2.22	0.33	2.15	0.31	20.90	0.73	0.40	3.63	0.65	5.8	1.0
GJP-67	WMK	Tonalite	1.72	4.61	0.71	4.21	0.87	2.53	0.35	2.43	0.34	23.98	0.95	0.41	1.96	0.42	5.9	1.2
GJP-68	WMK	Granodiorite	1.50	4.80	0.66	3.91	0.77	2.26	0.32	2.01	0.29	22.10	0.78	0.82	4.55	2.14	11.5	0.9

Notes: EI, Ecstall intrusives; WMK, western middle Cretaceous intrusives.

Table 2(a). Major elements (wt%) composition for samples on the eastern side of the Coastal Shear Zone.

Sample	Intrusive group	Petrology	Age (Ma)	SiO_2	TiO_2	Al_2O_3	$Fe_2O_3^*$	MnO	MgO	CaO	Na_2O	K_2O	P_2O_5	LOI	FeOt	Total	A/CNK
GJP-10	Ei	Granite	*52.7 ± 1.5*	72.63	0.19	15.49	1.23	0.03	0.35	1.98	5.05	2.63	0.06	0.33	1.11	99.95	1.05
GJP-11	Ei	Granite	*52.7 ± 1.5*	74.96	0.09	14.06	0.86	0.08	0.23	0.78	4.25	3.78	0.09	0.62	0.77	99.82	1.12
GJP-16	Ei	Granodiorite	52.7 ± 1.5	72.71	0.13	15.45	1.14	0.03	0.30	1.84	4.86	2.91	0.04	0.34	1.03	99.74	1.07
GJP-21	Ei	Granite	*52.7 ± 1.5*	72.10	0.13	15.58	1.36	0.04	0.25	1.86	5.10	3.08	0.04	0.27	1.22	99.81	1.03
GJP-82	Ei	Granite	49.8 ± 0.7	75.07	0.09	14.22	1.09	0.03	0.28	1.97	3.78	3.06	0.03	0.49	0.98	100.11	1.08
GJP-12	CSZ i	Granodiorite	58.4 ± 1.9	67.96	0.46	16.44	2.82	0.05	0.90	3.11	5.05	1.81	0.19	0.36	2.54	99.15	1.03
GJP-13	CSZ i	Granite	98.4 ± 1.8	69.52	0.27	15.87	2.47	0.06	0.87	3.61	4.39	1.59	0.10	0.36	2.22	99.12	1.02
GJP-14	CSZ i	Granodiorite	*58.4 ± 1.9*	61.26	0.99	16.35	6.17	0.09	2.57	4.98	4.28	1.95	0.35	0.50	5.55	99.47	0.90
GJP-77	CSZ i	Granodiorite	55.6 ± 0.7	70.02	0.41	15.98	2.55	0.03	0.77	3.18	4.64	1.73	0.16	0.31	2.29	99.78	1.05
GJP-79	CSZ i	Granodiorite	59.5 ± 1.7	62.10	0.84	16.54	5.50	0.08	2.81	5.49	4.05	1.64	0.25	0.60	4.95	99.90	0.90
GJP-84	CSZ i	Tonalite	60.9 ± 0.7	57.37	0.92	18.95	6.77	0.08	3.07	6.69	4.19	1.26	0.31	0.69	6.09	100.31	0.93
GJP-85	CSZ i	Granodiorite	59	57.83	0.97	16.97	7.13	0.11	4.03	6.32	3.59	1.96	0.34	0.40	6.42	99.65	0.87
GJP-23	ELK	Granite	82.8 ± 2.8	75.85	0.06	14.38	0.65	0.10	0.14	0.88	4.35	3.91	0.04	0.41	0.58	100.77	1.11
GJP-3	ELK	Granite	**72.0 ± 0.3**	72.68	0.20	14.98	1.97	0.06	0.60	2.49	4.62	2.17	0.08	0.34	1.77	100.19	1.03
GJP-4	ELK	Granite	**72.0 ± 0.3**	77.20	0.09	13.23	0.84	0.05	0.13	0.67	4.53	3.58	0.04	0.27	0.76	100.62	1.05
GJP-6	ELK	Granite	**72.0 ± 0.3**	61.81	0.79	17.62	6.38	0.31	1.90	2.33	5.71	2.50	0.29	0.53	5.74	100.15	1.08
GJP-8	ELK	Granodiorite	**68.2 ± 1.0**	60.72	0.85	16.53	6.59	0.10	2.97	5.90	4.15	2.01	0.29	0.22	5.93	100.32	0.84
GJP-9	ELK	Granodiorite	77.3 ± 1.7	66.43	0.46	16.02	3.76	0.07	1.65	3.56	4.52	2.36	0.15	1.57	3.38	100.53	0.97
GJP-22	ELK	Granodiorite	61.5 ± 1.7	63.10	0.64	17.27	4.77	0.09	2.20	4.90	4.45	1.94	0.19	0.48	4.29	100.04	0.94
GJP-78	ELK	Granodiorite	85	63.34	0.50	17.71	4.83	0.11	1.93	5.19	4.34	1.50	0.25	0.34	4.35	100.05	0.97
GJP-86	ELK	Granodiorite	81.9 ± 1.1	56.11	0.93	17.50	7.39	0.12	4.46	7.00	3.92	1.64	0.32	0.68	6.65	100.07	0.84
GJP-90	ELK	Granodiorite	52	67.36	0.27	16.72	2.59	0.08	1.12	3.84	4.44	2.22	0.14	0.74	2.33	99.51	1.00

Notes: Ei, Eocene intrusives; CSZ i, Coastal Shear Zone intrusives; ELK, eastern Late Cretaceous intrusives. Samples with italicized ages are extrapolated from adjacent dated samples of the same intrusive body or suite as determined by observed field relationships. Bold ages are derived from Mahoney *et al.* (in press) from samples of the same intrusive bodies.

Table 2(b). Trace elements (ppm) composition for samples on the eastern side of the Coastal Shear Zone.

Sample	Intrusive group	Petrology	Ba	Rb	Sr	Zr	Nb	Ni	Co	Zn	Cr	Th	Ce	Pr	Nd	Sm
GJP-10	Ei	Granite	940.03	61.81	638.33	79.23	2.29	0.88	1.63	125.91	2.32	27.98	58.14	7.42	28.20	5.12
GJP-11	Ei	Granite	917.42	71.42	148.12	37.66	8.99	1.43	0.87	93.08	9.20	13.06	25.86	3.04	10.92	2.17
GJP-16	Ei	Granodiorite	1344.77	71.20	673.85	65.16	2.13	2.38	1.44	83.72	9.66	7.04	14.24	1.71	6.72	1.33
GJP-21	Ei	Granite	1572.84	65.59	622.80	70.67	2.87		2.10	95.73	6.92	10.07	16.52	2.00	7.69	1.57
GJP-82	Ei	Granite	2356.03	45.18	511.82	33.51	2.41	1.67	1.04	34.62	7.79	11.40	22.57	2.76	10.29	1.83
GJP-12	CSZ i	Granodiorite	1130.30	34.83	806.64	118.55	3.95	2.98	5.38	124.95	8.25	53.90	104.40	11.83	41.20	5.84
GJP-13	CSZ i	Granite	2039.29	30.85	647.47	70.97	4.21	1.55	4.74	89.38	7.51	225.47	400.62	41.31	129.62	17.18
GJP-14	CSZ i	Granodiorite	881.92	36.97	883.38	102.73	6.98	10.90	15.26	123.15	24.37	14.22	39.11	5.84	25.70	5.43
GJP-77	CSZ i	Granodiorite	1086.08	33.97	865.49	144.92	4.55	1.36	4.29	48.62	6.10	20.91	38.82	4.45	15.13	2.43
GJP-79	CSZ i	Granodiorite	902.62	32.42	823.86	134.57	7.31	9.42	15.05	79.64	47.81	15.42	35.59	4.74	18.54	3.62
GJP-84	CSZ i	Tonalite	670.52	25.13	1108.40	214.98	4.95	9.55	19.21	92.92	39.64	8.66	20.70	3.16	14.35	3.40
GJP-85	CSZ i	Granodiorite	1027.78	46.45	781.32	117.30	6.44	15.82	23.19	93.29	78.47	30.53	60.65	7.02	25.50	4.47
GJP-23	ELK	Granite	1015.20	79.49	130.97	47.25	9.93		0.43	83.23	1.86	11.60	24.99	3.08	11.13	2.32
GJP-3	ELK	Granite	1483.35	28.94	378.85	59.01	2.70	3.17	3.38	109.02	9.54	14.10	25.31	2.97	10.71	1.93
GJP-4	ELK	Granite	665.41	73.30	117.14	48.83	8.03	1.87	0.63	70.74	9.46	11.50	23.47	2.78	9.43	2.07
GJP-6	ELK	Granite	398.58	130.59	297.27	123.20	21.86	2.81	10.24	262.71	11.65	32.08	71.39	8.90	32.68	8.20
GJP-8	ELK	Granodiorite	681.91	55.13	621.00	178.02	5.90	14.33	20.56	140.79	30.54	17.06	40.13	5.49	22.98	5.01
GJP-9	ELK	Granodiorite	981.29	44.13	578.53	75.03	5.41	10.21	10.44	119.67	27.45	21.39	38.84	4.47	16.42	3.10
GJP-22	ELK	Granodiorite	934.99	39.28	855.30	61.13	4.53	6.30	12.24	109.44	16.28	22.74	44.33	5.06	18.59	3.27
GJP-78	ELK	Granodiorite	997.94	38.60	772.63	156.72	6.73	7.12	10.00	63.61	18.88	34.72	67.77	7.85	27.34	4.62
GJP-86	ELK	Granodiorite	663.16	39.49	785.65	85.67	5.71	40.72	25.52	88.07	120.18	12.47	31.07	4.63	20.03	4.65
GJP-90	ELK	Granodiorite	1801.52	67.11	1037.68	96.54	6.85	6.75	6.49	48.04	19.40	11.74	23.17	3.07	12.27	2.60

Notes: Ei, Eocene intrusives; CSZ i, Coastal Shear Zone intrusives; ELK, eastern Late Cretaceous intrusives.

Table 2(c). Trace elements (ppm) composition for samples on the eastern side of the Coastal Shear Zone.

Sample	Intrusive group	Petrology	Eu	Gd	Tb	Dy	Ho	Er	Tm	Yb	Lu	Y	Cs	Ta	Hf	U	La/Yb	Eu/Eu*
GJP-10	Ei	Granite	0.71	3.51	0.29	1.32	0.17	0.39	0.04	0.28	0.04	4.53	1.78	0.24	2.69	0.55	98.2	0.5
GJP-11	Ei	Granite	0.46	1.95	0.30	1.82	0.33	0.91	0.13	0.83	0.11	9.29	1.80	0.74	1.51	0.63	15.8	0.7
GJP-16	Ei	Granodiorite	0.42	1.03	0.12	0.64	0.11	0.33	0.05	0.34	0.04	4.30	3.54	0.20	2.25	0.30	20.8	1.1
GJP-21	Ei	Granite	0.51	1.24	0.16	0.88	0.16	0.45	0.07	0.46	0.06	5.79	2.41	0.27	2.47	1.30	22.1	1.1
GJP-82	Ei	Granite	0.59	1.50	0.15	0.85	0.17	0.43	0.06	0.46	0.07	5.16	0.48	0.10	1.05	0.25	24.8	1.1
GJP-12	CSZ i	Granodiorite	1.15	3.41	0.27	1.08	0.15	0.33	0.04	0.26	0.03	4.94	0.57	0.09	3.51	0.23	208.9	0.7
GJP-13	CSZ i	Granite	3.41	10.41	0.85	3.55	0.54	1.22	0.15	0.97	0.14	13.97	0.47	0.20	2.24	1.24	232.2	0.7
GJP-14	CSZ i	Granodiorite	1.50	4.11	0.50	2.65	0.47	1.21	0.16	1.01	0.14	13.16	0.78	0.54	3.06	0.81	14.0	0.9
GJP-77	CSZ i	Granodiorite	0.90	1.89	0.19	0.96	0.18	0.45	0.06	0.43	0.05	6.73	0.43	0.20	3.98	0.43	48.2	1.2
GJP-79	CSZ i	Granodiorite	1.18	3.22	0.39	2.14	0.38	1.02	0.14	0.97	0.12	11.90	0.71	0.42	3.60	0.80	15.9	1.0
GJP-84	CSZ i	Tonalite	1.20	3.05	0.41	2.15	0.38	1.03	0.14	0.92	0.12	12.39	0.40	0.22	5.26	0.63	9.4	1.1
GJP-85	CSZ i	Granodiorite	1.26	3.85	0.47	2.73	0.50	1.34	0.20	1.33	0.16	14.42	0.68	0.34	3.11	0.33	23.0	0.9
GJP-23	ELK	Granite	0.46	1.99	0.26	1.51	0.28	0.81	0.13	0.79	0.12	8.61	1.34	0.73	2.08	0.73	14.7	0.6
GJP-3	ELK	Granite	0.53	1.55	0.20	1.08	0.20	0.56	0.08	0.51	0.08	6.08	0.53	0.14	1.79	0.42	27.4	0.9
GJP-4	ELK	Granite	0.34	1.84	0.26	1.53	0.28	0.77	0.12	0.71	0.10	8.47	1.45	0.95	2.01	1.12	16.3	0.5
GJP-6	ELK	Granite	0.92	7.79	1.27	7.49	1.30	3.37	0.46	2.83	0.35	38.77	3.29	1.11	3.74	3.95	11.3	0.3
GJP-8	ELK	Granodiorite	1.22	4.58	0.61	3.38	0.64	1.83	0.26	1.61	0.22	18.04	2.32	0.33	5.10	1.58	10.6	0.8
GJP-9	ELK	Granodiorite	0.92	2.43	0.29	1.54	0.29	0.78	0.11	0.71	0.10	8.26	1.09	0.52	2.42	2.00	30.2	1.0
GJP-22	ELK	Granodiorite	0.97	2.85	0.32	1.76	0.30	0.81	0.11	0.73	0.09	9.35	1.45	0.45	1.84	1.30	31.3	0.9
GJP-78	ELK	Granodiorite	1.38	3.84	0.45	2.71	0.50	1.43	0.19	1.42	0.19	15.05	0.88	0.24	3.94	0.52	24.5	1.0
GJP-86	ELK	Granodiorite	1.49	4.25	0.60	3.32	0.64	1.77	0.25	1.67	0.23	18.30	0.96	0.30	2.37	0.97	7.5	1.0
GJP-90	ELK	Granodiorite	0.97	2.05	0.25	1.48	0.28	0.82	0.13	1.00	0.13	10.79	3.19	0.65	2.81	2.63	11.8	1.2

Notes: Ei, Eocene intrusives; CSZ i, Coastal Shear Zone intrusives; ELK, eastern Late Cretaceous intrusives.

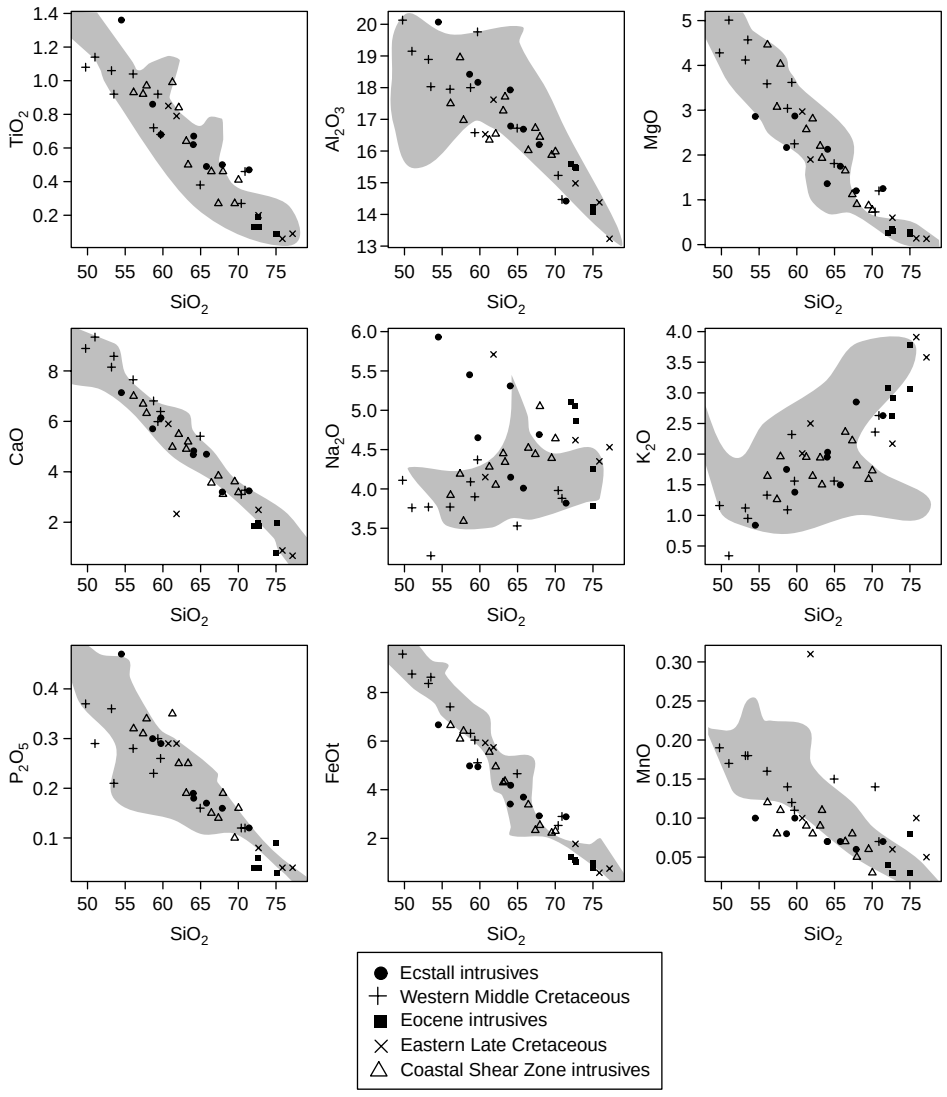

Figure 2. Major elements Harker plots of wt% TiO_2, Al_2O_3, MgO, CaO, Na_2O, K_2O, P_2O_5, FeOt, and MnO versus wt% SiO_2.

produced the Coast Mountains Batholith melts were grossly similar throughout the history and geography of this system. In particular, the well-defined, linear trends with substantial overlap for all intrusive suites observed in Figures 2 and 3 suggest that the Coast Mountains Batholith melts were all derived from broadly similar mafic crustal/lithospheric sources. In addition, they support the assertion that these melts also experienced comparable evolutions following extraction from their sources and limit the magnitude of involvement of melts or assimilants with dramatically diverse origins. On average, however, the eastern intrusive samples are slightly more silicic and peraluminous than those from west of the CSZ. Trace elemental compositions are also strikingly similar among the intrusive groups, where only Th exhibits consistent variability and to a lesser degree Ti (Figure 4). In particular, Th is elevated for all samples from east of the CSZ

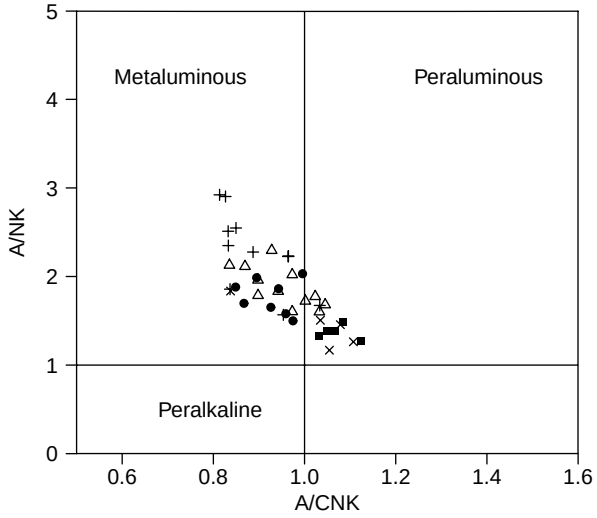

Figure 3. A/CNK (Al_2O_3/(CaO + Na_2O + K_2O), mol%) versus A/NK (Al_2O_3/(Na_2O + K_2O), mol%) diagram for discriminating metaluminous, peraluminous, and peralkaline compositions. Symbol designations match those from Figure 2.

relative to those from the west, but is most dramatically enriched in the CSZ and Eocene intrusives. Combined, the minor variations of the major and trace elemental compositions between the western and eastern samples likely reflect derivation of melts from greater crustal depth with higher grade metamorphic mineral assemblages for the source region of the eastern intrusives relative to the western intrusives (e.g. Figure 5). This results from local Palaeocene contraction and crustal thickening along the CSZ (Rusmore *et al.* 2001). Most intrusive suites also exhibit a minor Ti depletion with the Ecstall-equivalent intrusives representing the only exception. This likely reflects the slightly higher proportion of modal hornblende within the Ecstall-equivalent intrusives.

In a similar geochemical study of the Coast Mountains Batholith, Crawford *et al.* (2005) report major and trace elemental data from similar-age intrusives straddling the CSZ in an area ~150 km north of the northern transect investigated here. While their sampling did include a number of more mafic bodies, including synplutonic dikes, for the range of silica contents of the samples reported herein, there is almost complete overlap (Figure 2). The petrogenetic model described by Crawford *et al.* (2005) involves the melting of hydrated mantle with the modification of melts generated east of the CSZ by lower crustal melts of either continental composition and/or amphibolitic hydrated basalt. While data from this study support the interpretation that Coast Mountains Batholithic magmas, as with most arc magmas, were generated through a combination of mantle and lower crust-derived melts, they do not require or even strongly support a continental affinity for that lower crust. This follows from the observed uniform elemental, particularly trace elemental, compositions within and between individual intrusive groups (Figures 2 and 4). The composition of potentially contributing sources is discussed further in the next section. Mahoney *et al.* (in press) also report elemental and strontium isotopic data for Late Jurassic through Eocene intrusives east of the CSZ in the region surrounding Bella Coola and overlapping the eastern Dean–Burke Channel transect (Figure 1(b)) from this study. Data from their study also overlap our data from the intrusions east of the CSZ, which should not be surprising given that we have, in many cases, sampled the same

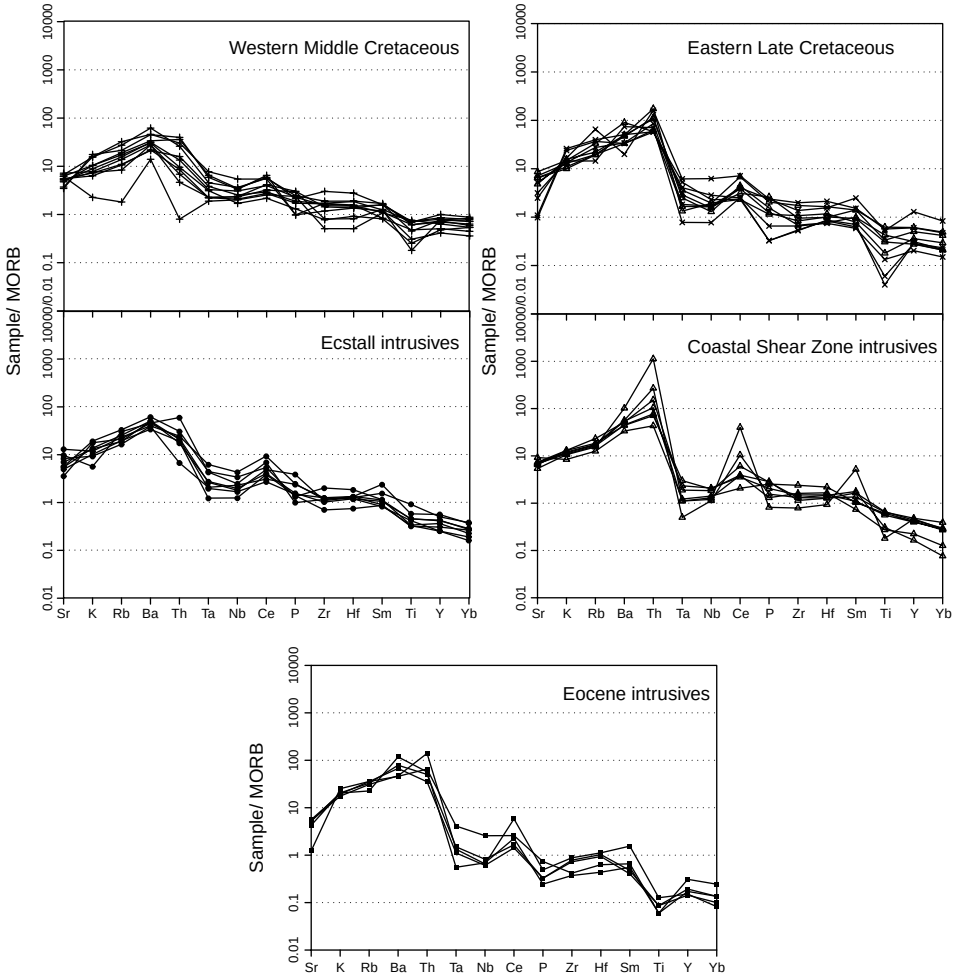

Figure 4. Rock/mid-ocean ridge basalt (MORB; data from Pearce 1983) normalized diagrams for the Coast Mountains Batholith intrusive groups.

intrusive bodies. They argue that the arc east of the CSZ underwent dramatic crustal thickening during the Late Cretaceous followed by an equally dramatic crustal thinning event, possibly associated with the delamination of a portion of the lower crust, during the Palaeocene to Eocene. These interpretations are generally supported by data present in this study, particularly the Late Cretaceous crustal thickening which can be documented on a broader regional scale on both sides of the CSZ (e.g. Figure 5).

Isotopic variations

The first fundamental result provided by the isotopic dataset reported here is that variations of the isotopic compositions of the Coast Mountains Batholith intrusives are minor with respect to composition, time, and geographic position. Furthermore, when compared with other Mesozoic batholiths of the North American Cordillera, the Coast Mountains Batholith correlates well with those of the western or outboard portions inasmuch as they are isotopically primitive with regard to radiogenic isotopes (e.g. Kistler and Peterman

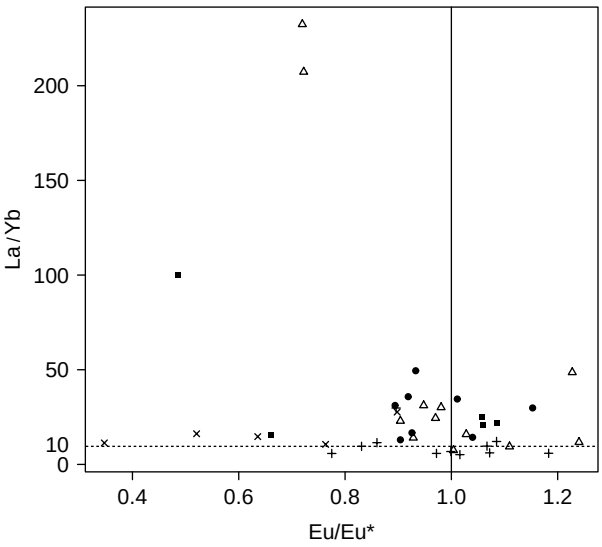

Figure 5. Eu/Eu* versus La/Yb correlation diagram for the Coast Mountains Batholith intrusive groups. Dashed horizontal line at La/Yb = 10 corresponds with an approximate crustal thickness of 30–35 km (Hildreth and Moorbath 1988). Symbol designations match those from Figure 2.

1978). Previous studies of the Coast Mountains Batholith (Magaritz and Taylor 1976, 1986; Barker *et al.* 1986; Arth *et al.* 1988; Samson *et al.* 1989, 1990, 1991a,b; Barker and Arth 1990; Cui and Russell 1995a,b; Friedman *et al.* 1995; Thomas and Sinha 1999; Mahoney *et al.* in press) have reported results similar to those reported herein. Clearly, the bulk of this arc has primitive radiogenic isotopic compositions, suggesting that North American lithosphere (mantle and crust) made only a relatively minor, if any contribution in generating the Coast Mountains Batholith melts.

Radiogenic isotopic compositions for both Pb and Sr are relatively consistent in terms of mean and variability (Figure 6(d),(f)). Eastern Late Cretaceous intrusives, however, do exhibit consistently lower Pb and Sr isotopic compositions than all other intrusive suites presented in this study. Slight variations in radiogenic isotopic compositions as a function of geographic position, for example distance from the CSZ (Figure 6(g),(i)), likely reflect the combined effects of spatial migration of magmatism through time combined with that of the focus of contraction and crustal thickening. For example, the low overall Sr and Pb isotopic compositions of samples from the eastern Late Cretaceous intrusives may reflect a greater mantle-derived component as a result of subdued crustal interaction, as these melts were emplaced through overall thinner crust ahead of Palaeocene contraction in this part of the Coast Mountains (Gehrels *et al.* 1992; McClelland *et al.* 1992; Journeay and Friedman 1993; Rusmore *et al.* 2000, 2005). Oxygen isotopes exhibit no clear trend as a function of time or geographic position with nearly the entire range of observed values present from all intrusive suites on both sides of the CSZ (Figure 6(e),(h)).

A comparison of our data with that from other parts of the Coast Mountains Batholith shows remarkable similarities. A plot of $^{207}Pb/^{204}Pb$ and $^{87}Sr/^{86}Sr$ against $^{206}Pb/^{204}Pb$ (Figure 7(a),(c)) demonstrates significant overlap between the Coast Mountains Batholith intrusives of this study and those of the southern Coast Mountains Batholith (Cui and Russell 1995a,b).

Table 3. Isotopic ratios of whole-rock samples (lead and strontium) and quartz separates (oxygen) of samples collected from the central Coast Mountains Batholith.

Sample	Intrusive group	$^{87}Sr/^{86}Sr$ measured	$^{87}Sr/^{86}Sr$ initial	$^{206}Pb/^{204}Pb$ measured	$^{207}Pb/^{204}Pb$ measured	$^{208}Pb/^{204}Pb$ measured	$^{206}Pb/^{204}Pb$ initial	$^{207}Pb/^{204}Pb$ initial	$^{208}Pb/^{204}Pb$ initial	$\delta^{18}O$
GJP-19	EI	0.70431	0.70420	19.087	15.602	38.505	18.984	15.597	38.329	
GJP-29	EI	0.70427	0.70410	19.011	15.611	38.546	18.782	15.600	38.379	7.2
GJP-32	EI	0.70473	0.70435	19.108	15.595	38.396	18.901	15.585	38.034	7.2
GJP-36	EI	0.70450	0.70433	19.024	15.587	38.448	18.855	15.579	38.318	8.8
GJP-44	EI	0.70464	0.70431	19.120	15.610	38.638	18.972	15.603	38.470	9.6
GJP-69	EI	0.70439	0.70427	19.107	15.614	38.562	18.953	15.607	38.495	9.2
GJP-71	EI	0.70465	0.70439	19.267	15.643	38.797	19.078	15.634	38.661	
GJP-83	EI	0.70417	0.70394	18.898	15.563	38.448	18.836	15.560	38.271	
GJP-37	WMK	0.70389	0.70366	19.148	15.580	38.413	18.846	15.566	37.877	7.1
GJP-38	WMK	0.70389	0.70375	18.801	15.564	38.299	18.646	15.556	38.157	
GJP-39	WMK	0.70579	0.70534	19.317	15.604	38.910	19.072	15.592	38.627	8.6
GJP-40	WMK	0.70419	0.70394	18.841	15.571	38.499	18.685	15.564	38.406	8.9
GJP-43	WMK	0.70422	0.70419	18.784	15.575	38.263	18.748	15.574	38.243	6.8
GJP-62	WMK	0.70500	0.70486	18.957	15.586	38.469	18.630	15.570	38.206	
GJP-63	WMK	0.70500	0.70480	18.890	15.582	38.388	18.738	15.575	38.267	
GJP-64	WMK	0.70520	0.70456	18.979	15.564	38.273	18.586	15.545	38.044	10.0
GJP-65	WMK	0.70429	0.70416	18.858	15.565	38.295	18.687	15.557	38.153	
GJP-67	WMK	0.70407	0.70397	18.737	15.553	38.231	18.622	15.548	38.150	
GJP-68	WMK	0.70478	0.70451	19.166	15.612	38.683	18.931	15.601	38.500	
GJP-10	Ei	0.70438	0.70417	18.928	15.598	38.476	18.909	15.597	38.407	
GJP-11	Ei	0.70562	0.70458	19.035	15.585	38.325	19.009	15.584	38.247	
GJP-16	Ei	0.70467	0.70444	18.940	15.600	38.518	18.930	15.599	38.502	9.5
GJP-21	Ei	0.70443	0.70420	18.969	15.614	38.534	18.927	15.612	38.513	
GJP-82	Ei	0.70464	0.70447	19.030	15.592	38.485	19.019	15.591	38.458	7.9
GJP-12	CSZ i	0.70429	0.70418	18.875	15.582	38.502	18.858	15.581	38.310	9.0
GJP-13	CSZ i	0.70437	0.70418	19.013	15.603	38.957	18.865	15.596	37.115	
GJP-14	CSZ i	0.70393	0.70383	18.861	15.585	38.416	18.785	15.581	38.366	
GJP-77	CSZ i	0.70450	0.70441	18.898	15.578	38.465	18.869	15.576	38.404	7.9
GJP-79	CSZ i	0.70493	0.70484	18.927	15.591	38.529	18.867	15.589	38.477	7.5
GJP-84	CSZ i	0.70461	0.70455	18.930	15.602	38.481	18.867	15.599	38.457	

Table 3 – *continued*

Sample	Intrusive group	$^{87}Sr/^{86}Sr$ measured	$^{87}Sr/^{86}Sr$ initial	$^{206}Pb/^{204}Pb$ measured	$^{207}Pb/^{204}Pb$ measured	$^{208}Pb/^{204}Pb$ measured	$^{206}Pb/^{204}Pb$ initial	$^{207}Pb/^{204}Pb$ initial	$^{208}Pb/^{204}Pb$ initial	$\delta^{18}O$
GJP-85	CSZ i	0.70478	0.70464	18.923	15.595	38.489	18.890	15.593	38.337	
GJP-3	ELK	0.70374	0.70351	18.736	15.567	38.344	18.695	15.565	38.264	
GJP-4	ELK	0.70534	0.70349	18.843	15.576	38.433	18.786	15.573	38.347	
GJP-6	ELK	0.70478	0.70348	18.962	15.584	38.506	18.624	15.568	38.253	
GJP-8	ELK	0.70385	0.70360	18.899	15.587	38.464	18.784	15.581	38.330	
GJP-9	ELK	0.70371	0.70347							9.8
GJP-22	ELK	0.70413	0.70402	18.848	15.591	38.402	18.755	15.587	38.301	8.9
GJP-23	ELK	0.70546	0.70340	18.797	15.577	38.296	18.754	15.575	38.223	8.4
GJP-78	ELK	0.70370	0.70352	18.849	15.578	38.425	18.772	15.575	38.038	7.0
GJP-86	ELK	0.70408	0.70391	18.942	15.596	38.454	18.811	15.590	38.418	
GJP-90	ELK	0.70381	0.70367	18.752	15.550	38.155	18.655	15.545	38.120	

Notes: EI, Ecstall intrusives; WMK, western middle Cretaceous intrusives; Ei, Eocene intrusives; CSZ i, Coastal Shear Zone intrusives; ELK, eastern Late Cretaceous intrusives.

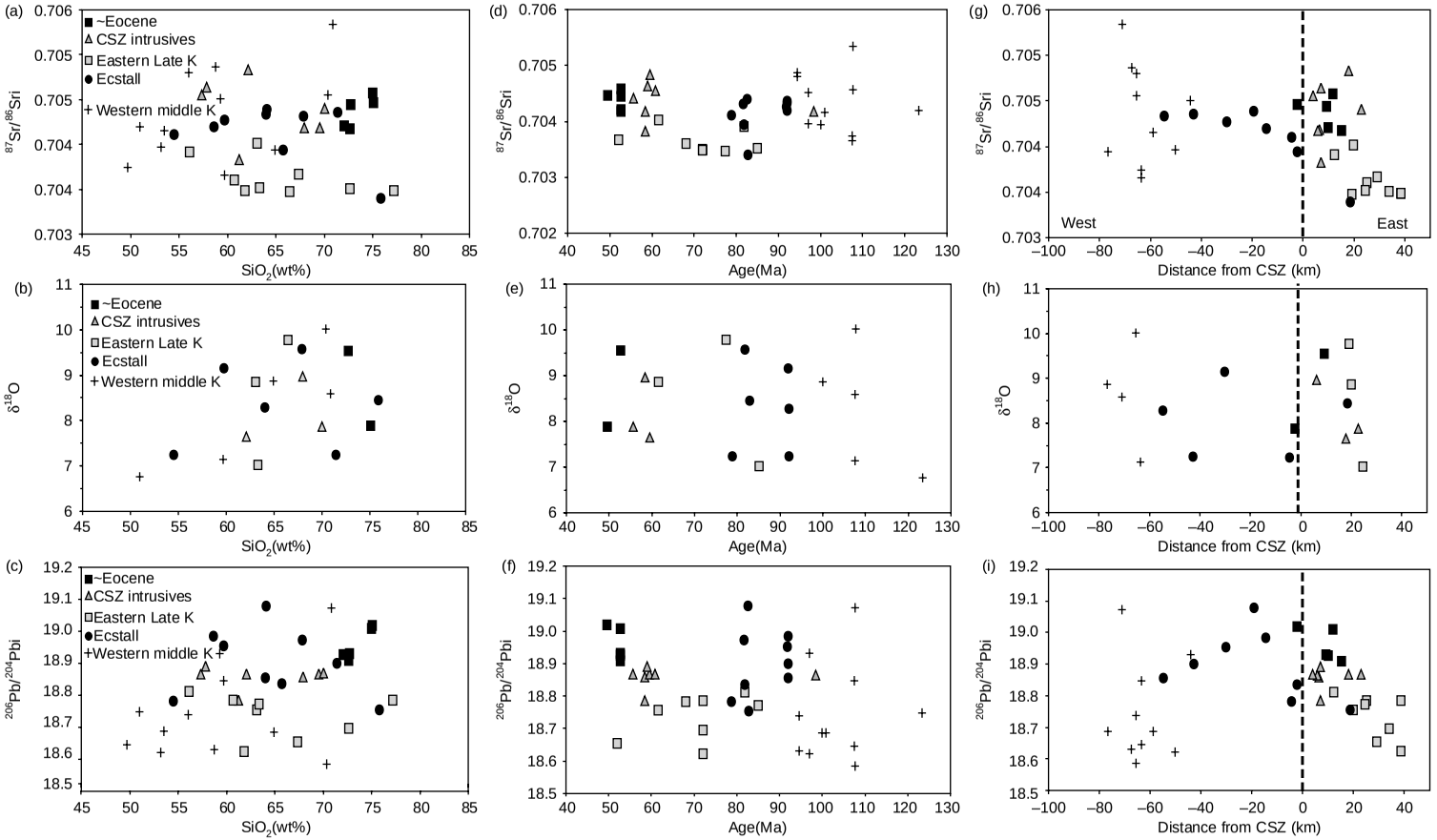

Figure 6. (a) Plot of $^{87}Sr/^{86}Sr$ versus SiO_2. (b) Plot of $\delta\ ^{18}O$ versus SiO_2. (c) Plot of $^{206}Pb/^{204}Pb$ versus SiO_2. (d) Plot of $^{87}Sr/^{86}Sr$ versus age. (e) Plot of $\delta\ ^{18}O$ versus age. (f) Plot of $^{206}Pb/^{204}Pb$ versus age. (g) Plot of $^{87}Sr/^{86}Sr$ versus distance from the CSZ. (h) Plot of $\delta\ ^{18}O$ versus distance from the CSZ. (i) Plot of $^{206}Pb/^{204}Pb$ versus distance from the CSZ.

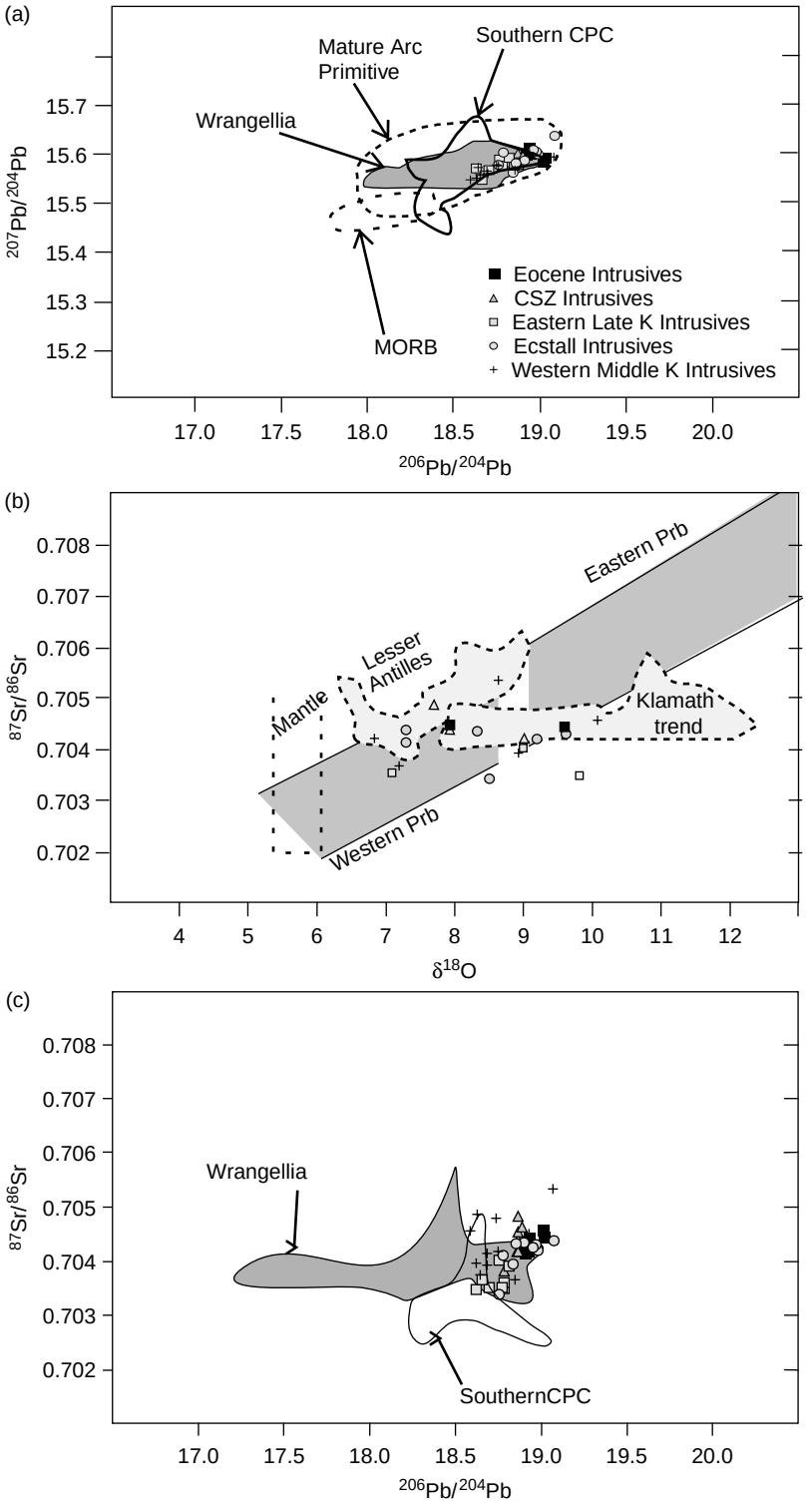

Oxygen isotopic data (quartz) from intrusives of the central Coast Mountains Batholith range from 6.8 to 10.0‰, with a mean value of 8.4‰. No trends are apparent from these data with respect to geographic position, age of intrusive body sampled, or composition (e.g. wt% SiO_2; Figure 6(b)). These data overlap with those of Magaritz and Taylor (1976) from their zones I and II and from Gehrels and Taylor (1984) in the Ketchikan area, both to the north of the study area reported on herein. These data also overlap with oxygen data reported from the southern Coast Mountains Batholith (Magaritz and Taylor 1986).

A comparison of the strontium and oxygen data with the Peninsular Ranges batholith of southern and Baja California (Taylor 1986) reveals partial overlap with the primitive western Peninsular Ranges batholith (Figure 7(b)). However, several of the samples from this study display higher oxygen values for samples with equivalent $^{87}Sr/^{86}Sr_i$ ratios from the Peninsular Ranges batholith. Heavy oxygen in excess of the Peninsular Ranges batholith trend is observed in four out of five of the intrusive belts from both sides of the CSZ. The observation of excessively heavy oxygen signatures is relatively rare but is observed elsewhere in the Cordillera. Barnes *et al.* (1990) report a similar heavy oxygen excursion from the intrusives of the Klamath Mountains (Figure 7(b)). They argue that the unique isotopic composition of the Klamath magmas arises from the assimilation of metavolcanics and volcaniclastics with slightly elevated strontium isotopes ($^{87}Sr/^{86}Sr_i \sim 0.705$) but very heavy oxygen ($\delta\,^{18}O > 10.5$‰).

In summary, Coast Mountains Batholith intrusive belts are characterized by relatively uniform radiogenic isotopic compositions, internally and from one belt to the next, regardless of petrologic composition, age, or geographic position. Slightly less radiogenic compositions for the eastern Late Cretaceous intrusives likely reflect less interaction with a crustal column that was thinner relative to those encountered by other intrusive suites during magma ascent. Nevertheless, the Coast Mountains Batholith intrusives are overall primitive, but isotopically slightly more evolved than typical island arcs, e.g. Lesser Antilles arc (Figure 7(b)). Oxygen isotopes are particularly anomalous when compared with the outboard portions (i.e. those parts with similar radiogenic isotopic compositions) of almost every other Mesozoic to Cenozoic batholith in the North American Cordillera. We believe that these data suggest a unique history to the source rocks of the Coast Mountains Batholith.

Discussion

Elemental and isotopic data presented here demonstrate that there is a significant mantle-wedge-derived component to the batholith, which is expected for any magmatic arc. In addition, we identify a second, heavy oxygen component, whose origin is examined in detail below.

The elevated quartz $\delta\,^{18}O$ values for the Coast Mountains Batholith samples (from 6.8 to 10.0‰) clearly suggest that the batholithic source(s) contains a significant fraction of rocks that were previously at or near the surface of the Earth. Mafic rocks derived from partial

Figure 7. (a) Pb–Pb plot illustrating various tectonic fields after Zartman and Doe (1981) as well as data from the southern CPC (Cui and Russell 1995a,b) and Wrangellia (Andrew and Goodwin 1989a,b). (b) Sr versus $\delta\,^{18}O$ plot comparing data from the CPC with the Peninsular Ranges batholith (Taylor 1986), the Lesser Antilles arc (Davidson and Harmon 1989), and the Klamath trend (Barnes *et al.* 1990). (c) Sr versus Pb plot comparing data from the CPC with data from the southern CPC (Cui and Russell 1995a,b) and Wrangellia (Andrew and Goodwin 1989a,b).

melting of the mantle have a global average $\delta\ ^{18}O = 5.7 \pm 0.3‰$ (Mattey *et al.* 1994; Harmon and Hoefs 1995), and even the most extreme crystal fractionation to a high-silica rhyolite cannot increase that ratio by more than 1‰ (Taylor and Sheppard 1986). Quartz $\delta\ ^{18}O$ is higher by a few tens of per mille ($\sim 0.5‰$) compared with whole-rock values. Overall, it has been established that any plutonic rock with quartz $\delta\ ^{18}O > 7‰$ must be derived at least in part from source rocks that were in contact with the hydrosphere at some point in their past, i.e. rocks that have a supracrustal history. These numbers assume that the analysed samples themselves experienced no hydrothermal or surficial alteration, or other open-system disturbance subsequent to the crystallization of the original magmatic rock. It is unusual for large volumes of crustal rocks to have $\delta\ ^{18}O > 12–14‰$ (Taylor 1986). Mass balance is straightforward with respect to oxygen isotopes, given that almost all minerals and rocks have about 50% oxygen by mass. The consequence is that a quartz $\delta\ ^{18}O = 8.4$, the average of the 19 measurements presented in this study, requires significant input from a crustal component, tens of per cent, depending on the $\delta\ ^{18}O$ composition of that component. The few measurements of quartz $\delta\ ^{18}O \sim 7‰$ (Figure 7(b)), on the other hand, are perfectly consistent with an unaltered mantle origin for the source rocks of the batholith melts. We interpret that component to represent the lower crustal intrusions derived from mantle wedge beneath the arc.

Using a conservative value of $\delta\ ^{18}O = 14‰$ for the near-surface component, and intrusive volume data from the area (Gehrels *et al.* in press), we estimate that about 40–45% of the volume of the studied plutons had to be derived from this component with elevated $\delta\ ^{18}O$. This is significant in that it rules out an exclusively *in situ* mantle-wedge-derived origin for these giant arc-related intrusions, some of the largest individual plutons in the world.

On an $^{87}Sr/^{86}Sr$ versus $\delta\ ^{18}O$ diagram (Figure 7(b)), the positive correlation commonly seen between isotopes in Cordilleran batholiths (e.g. Taylor 1986) is evident; high $\delta\ ^{18}O$ (10‰) values are associated with a minimal increase in $^{87}Sr/^{86}Sr$ to about 0.7045. The scatter observed in our data in this and other isotopic correlation diagrams might indicate multi-component mixing of at least three contributors, as it is the case with other batholiths (e.g. Ducea 2001). Of these various components, we can identify the most significant contributors by mass: a low $^{87}Sr/^{86}Sr$, lead and $\delta\ ^{18}O$ component as being unambiguously a mantle component (the mantle wedge beneath the Mesozoic arc), and the 'near-surface', high $\delta\ ^{18}O$ component. The high $\delta\ ^{18}O$ mass had to have been buried to deep crustal levels before becoming a significant component in the mass of the batholith.

What makes the Coast Mountains Batholith particularly interesting is that high $\delta\ ^{18}O$ values are found for rocks that have non-radiogenic Sr and Pb isotopes (as well as high ε_{Nd} isotopes; Girardi *et al.* 2009). In order to explain the origin of this 'surficial' component, one has to envision a crustal source rock that satisfies the following conditions: (1) it has to be a mafic to intermediate material in order to generate an I-type calc-alkaline suite by partial melting, (2) it has to be volumetrically significant, given the size of the batholith, (3) it has to be primitive in radiogenic isotopic compositions (island arc, oceanic plateau, etc.), and (4) it has to have experienced extensive low-temperature, near-surface interactions with meteoric and/or sea water, and consequently is a wet source.

Petrogenetic and tectonic implications

The above discussion places constraints on the composition, origin, and evolution of the source rocks that produced the melts of the Coast Mountains Batholith. We propose that the bulk of the batholith's lower crust evolved from a former large oceanic plateau

or at least Jurassic, if not older, relict island arc within the Pacific realm. Radiogenic isotopes, particularly common lead values, are more consistent with an island arc origin than an oceanic plateau. Amphibolite is the most likely composition of a wet basalt or basaltic andesite in the lower crust. There are, therefore, three potential origins for rocks with this unique composition and evolution to have been positioned in the lower crust of the Coast Mountains Batholith: (1) Jurassic and older arc rocks that were buried into a lower crustal position by the accumulation of igneous and sedimentary strata, (2) subduction erosion and underplating of accretionary prism and/or forearc blocks, and (3) accretion and post-accretion contractional deformation and crustal thickening.

The possibility that the source rocks of the Coast Mountains Batholith were buried Jurassic and older arc rocks may be a valid interpretation due to the presence of latest Proterozoic through mid to late Palaeozoic intrusive bodies and orthogneisses present within the study area (Boghossian and Gehrels 2000; Gareau and Woodsworth 2000; Gehrels and Boghossian 2000). However, this seems unlikely due to the presence of these units along with other Palaeozoic metasedimentary units at the surface today adjacent to the middle to upper crustal (2–5 kbar) intrusions of the Coast Mountains Batholith, as much as 7–8 kbar from the inferred depths of melt generation (Stowell and Crawford 2000; Brady, R. written communication, 2005).

Subduction erosion and underplating of forearc or accretionary prism blocks is also a potentially valid interpretation since contractional deformation dominated the late Early Cretaceous through earliest Tertiary arc at this latitude. Similarly, these tectonic features are not known to be preserved for this arc during this time period. Subduction erosion of the forearc may be an ideal mechanism responsible for at least some of the Coast Mountains Batholith melts, particularly if the eroded forearc blocks comprise crustal sections from outboard terranes such as Wrangellia. Similar to the Central American example described by Goss and Kay (2006), the mafic lithologies and isotopic geochemical compositions of Wrangellia (e.g. Figure 7(a),(c)) could produce the batholitic melts (discussed further below). However, for such a mechanism to be solely responsible for the generation of the Coast Mountains Batholith within the study area, it would require multiple, discrete erosional events over the course of $\sim$60 million years, a scenario that seems unlikely given the volume of melt produced and the possibility of alternative, and perhaps more plausible mechanisms.

Accretion and post-accretion contraction is, perhaps, the most appropriate mechanism for emplacing large volumes of upper-crustal rocks at depth and within the region of melt generation. The western Coast Mountains, which includes the Alexander and Wrangellia terranes, is interpreted to have been juxtaposed with the eastern Coast Mountains through a combination of sinistral translation and contraction during the Early to middle Cretaceous (McClelland *et al.* 1992; Monger *et al.* 1994; Gehrels *et al.* in press). Throughout the Coast Mountains are multiple individual faults/ductile shear zones, forming a west-vergent thrust belt, that were active from the late Early Cretaceous to the early Tertiary (Gehrels *et al.* 1992; McClelland *et al.* 1992; Journeay and Friedman 1993; Monger *et al.* 1994; Andronicos *et al.* 1999, 2003; Rusmore *et al.* 2000; Stowell and Crawford 2000). The magnitude of shortening accommodated by these west-vergent faults is poorly constrained; however, exposed footwall blocks do yield peak metamorphic pressures in excess of 7 kbar (Rusmore *et al.* 2005). In addition to the east of the Coast Mountains was the east-vergent Skeena Fold Belt, active from the latest Jurassic to early Tertiary, accommodating as much as 160 km of shortening (Evenchick 1991a,b, 2001). Both systems of thrusts would have funnelled crustal rocks to depths in excess of 35 km beneath the Coast Mountains Batholith triggering the kind of flare-up magmatism

(cf. Ducea and Barton 2007) characteristic of the central Coast Mountains during the middle Cretaceous through early Tertiary. More important, however, is the fact that the composition of the rocks being emplaced within the region of arc melt generation was compositionally appropriate to generate, not only the lithologies observed in the Coast Mountains Batholith, but also the isotopic compositions. The Wrangellia terrane, in particular comprises a large proportion of mafic volcanic rocks with isotopic geochemical compositions that overlap those of the Coast Mountains Batholith (Barker *et al.* 1986; Arth *et al.* 1988; Andrew and Goodwin 1989a,b; Samson *et al.* 1989, 1990, 1991a,b; Barker and Arth 1990; Lassiter *et al.* 1995; Figure 3(a),(c)). Hollister and Andronicos (2006) have independently proposed a similar tectonic model based on geologic and seismic data collected by project ACCRETE. The Central Gneiss Complex makes up the core of the Late Cretaceous and Cenozoic sections of the batholith at the latitude of this study and consists primarily of amphibolite (metamorphosed mafic volcanics) and metasedimentary rocks (Armstrong and Runkle 1979; Hollister and Andronicos 2000). The Central Gneiss has been suggested as the source for some of the intrusions of the Coast Mountains Batholith (e.g. Smith *et al.* 1979) and may be a part of this underthrust domain, which has subsequently been exhumed at the surface.

The existence of a regionally extensive high $\delta^{18}O$ component in the source of what is from a radiogenic isotope perspective a primitive magmatic arc (Samson *et al.* 1989, 1990, 1991a,b; Samson and Patchett 1991) has some important implications for the assembly of granitic crust in general. It is well established that making granitoids is a two-step process that requires either dramatic fractionation of mantle-derived basaltic melts or remelting of underplated or intruded mantle-derived melts (Rudnick 1995). The details of the second stage process are largely unresolved, but it has been proposed that remelting of newly underplated/intruded basalt in the lower crust can be responsible for the two-step process of generating granitoids (e.g. Atherton and Petford 1993). The Coast Mountains Batholith could be a perfect candidate for this process, given that most of its rocks have Phanerozoic Nd crustal ages (Samson *et al.* 1989, 1990, 1991a,b; Samson and Patchett 1991). However, the presence of the high $\delta^{18}O$ component in the batholith precludes this simple two-step process (melting in the mantle, basalt ponding in the lower crust, and remelting of basalts to make granitoids). It shows that even in the case of one of the most primitive Cordilleran batholiths (as documented by radiogenic isotopes), tectonic processes such as crustal thickening represent an integral part of arc evolution.

Conclusions

The petrologic, geochemical, and radiogenic isotopic composition of the Coast Mountains Batholith of west-central British Columbia, Canada, is similar to that of the western portions of the other North American Cordilleran batholiths. The various intrusive groups investigated and reported upon herein are characteristically calc-alkaline, metaluminous to weakly peraluminous, and isotopically juvenile. Oxygen isotopes, however, are uncharacteristically heavy for their radiogenic isotopic compositions, an observation that is not related to post-emplacement alteration as demonstrated by the petrographic characteristics of the analysed samples. Anomalously heavy oxygen compositions are observed in most of the intrusive groups investigated in this study suggesting a process/source that is both regionally and temporally extensive. Furthermore, they preclude the possibility that the Coast Mountains Batholithic melts were exclusively generated from the Mesozoic mantle wedge, just as the Sr and Pb data preclude significant involvement of an old (Precambrian) crustal/mantle lithospheric source. We interpret the

high $\delta^{18}O$ component to represent materials that had a multi-stage crustal evolution. They were originally mafic rocks derived from a circum-Pacific juvenile mantle wedge that experienced a period of near-surface residence after initial crystallization. During this interval, these primitive rocks interacted with meteoric waters at low temperatures, as indicated by the high $\delta^{18}O$ values. Subsequently, these materials were buried to lower crustal depths where they remelted to form the high $\delta^{18}O$ component of the Coast Mountains Batholith. A prolonged period of contractional deformation, beginning with the Early Cretaceous collisional accretion of the Insular superterrane, is inferred to have been responsible for underthrusting the high $\delta^{18}O$ component into the lower crust. We suggest that rocks of the Insular superterrane (e.g. Alexander–Wrangellia) are of ideal composition, and were accreted to and overthrust by what would become the Coast Mountains Batholith just prior to initiation of magmatism in that region.

Acknowledgements

This research was funded by NSF grant EAR-0309885 (Continental Dynamics). We are indebted to Mark Baker for assistance in sample preparation and ICP mass spectrometry. We thank George Gehrels and P. Jonathan Patchett for their assistance with sample collection and discussions that helped improved this manuscript. We thank Theresa Kayzar and Kelley Stair with laboratory help in the early stages of this project. We also thank Tyler Vandruff and Chao Li for their help with oxygen isotopic analyses at Arizona and Vio Atudorei for with oxygen isotopic analyses at New Mexico. The manuscript greatly benefited from constructive reviews by Brian Mahoney and Rick Carlson.

References

Andrew, A., and Godwin, C., 1989a, Lead- and strontium-isotope geochemistry of Paleozoic Sicker Group and Jurassic Bonanza Group volcanic rocks and Island Intrusions, Vancouver Island, British Columbia: Canadian Journal of Earth Sciences, v. 26, p. 894–907.

Andrew, A., and Godwin, C., 1989b, Lead- and strontium-isotope geochemistry of the Karmutsen Formation, Vancouver Island, British Columbia: Canadian Journal of Earth Sciences, v. 26, p. 908–919.

Andronicos, C.L., Chardon, D.H., Hollister, L.S., Gehrels, G.E., and Woodsworth, G.J., 2003, Strain partitioning in an obliquely convergent orogen, plutonism, and synorogenic collapse: Coast Mountains Batholith, British Columbia, Canada: Tectonics, v. 22, no. 1012, doi: 10.1029/2001TC001312.

Andronicos, C.L., Hollister, L.S., Davidson, C., and Chardon, D., 1999, Kinematics and tectonic significance of transpressive structures within the Coast Plutonic Complex, British Columbia: Journal of Structural Geology, v. 21, p. 229–243.

Annen, C., Blundy, J.D., and Sparks, R.S.J., 2006, The genesis of intermediate and silicic magmas in deep crustal hot zones: Journal of Petrology, v. 47, no. 3, p. 505–539.

Arculus, R.J., 1994, Aspects of magma genesis in arcs: Lithos, v. 33, p. 189–208.

Armstrong, R.L., and Runkle, D., 1979, Rb–Sr Geochronometry of the Ecstall, Kitkiata, and Quottoon Plutons and their Country Rocks, Prince Rupert Region, Coast Plutonic Complex, British-Columbia: Canadian Journal of Earth Sciences, v. 16, no. 3, p. 387–399.

Arth, J.G., Barker, F., and Stern, T.W., 1988, Coast Batholith and Taku plutons near Ketchikan, Alaska: Petrography, geochronology, geochemistry, and isotopic character: American Journal of Science, v. 288-A, p. 461–489.

Atherton, M.P., and Petford, N., 1993, Generation of sodium-rich magmas from newly underplated basaltic crust: Nature, v. 362, p. 144–146.

Barker, F., and Arth, J.G., 1990, Two traverses across the Coast batholith, southeastern Alaska, *in* Anderson, J.L., ed., The nature and origin of Cordilleran magmatism: Boulder, CO, Geological Society of America, p. 395–405.

Barker, F., Arth, J.G., and Stern, T.W., 1986, Evolution of the Coast Batholith Along the Skagway Traverse, Alaska and British-Columbia: American Mineralogist, v. 71, nos. 3–4, p. 632–643.

Barnes, C.G., Allen, C.M., Hoover, J.D., and Brigham, R.H., 1990, Magmatic components of a tilted plutonic system, Klamath Mountains, California, *in* Anderson, J.L., ed., The nature and origin of Cordilleran magmatism: Boulder, CO, Geological Society of America, p. 331–346.

Boghossian, N.D., and Gehrels, G.E., 2000, Nd isotopic signature of metasedimentary pendants in the Coast Mountains Between Prince Rupert and Bella Coola, British Columbia, *in* Stowell, H.H., and McClelland, W.C., eds., Tectonics of the Coast Mountains, southeastern Alaska and British Columbia: Boulder, CO, Geological Society of America, p. 77–87.

Butler, R.F., Gehrels, G.E., Baldwin, S.L., and Davidson, C., 2002, Paleomagnetism and geochronology of the Ecstall pluton in the Coast Mountains of British Columbia: Evidence for local deformation rather than large-scale transport: Journal of Geophysical Research, v. 107, doi: 10.1029/2001JB000270.

Chen, J.H., and Tilton, G.R., 1991, Applications of lead and strontium isotopic relationships to the petrogenesis of granitoid rocks, central Sierra Nevada batholith, California: Geological Society of America Bulletin, v. 103, p. 439–447.

Crawford, M.L., Crawford, W.A., and Gehrels, G.E., 2000, Terrane assembly and structural relationships in the eastern Prince Rupert quadrangle, British Columbia, *in* Stowell, H.H., and McClelland, W.C., eds., Tectonics of the Coast Mountains, southeastern Alaska and British Columbia: Boulder, CO, Geological Society of America, p. 1–21.

Crawford, M.L., Crawford, W.A., and Lindline, J., 2005, 105 Million years of igneous activity, Wrangell, Alaska, to Prince Rupert, British Columbia: Canadian Journal of Earth Sciences, v. 42, no. 6, p. 1097–1116.

Cui, Y., and Russell, J.K., 1995a, Magmatic origins of calc-alkaline intrusions from the Coast Plutonic Complex, southwestern British Columbia: Canadian Journal of Earth Sciences, v. 32, no. 10, p. 1643–1667.

Cui, Y., and Russell, J.K., 1995b, Nd–Sr–Pb isotopic studies of the southern Coast Plutonic Complex, southwestern British Columbia: Geological Society of American Bulletin, v. 107, no. 2, p. 127–138.

Davidson, J.P., and Harmon, R.S., 1989, Oxygen istope constraints on the petrogenesis of volcanic arc magmas from Martinique, Lesser Antilles: Earth and Planetary Science Letters, v. 95, p. 255–270.

DeCelles, P.G., Ducea, M.N., Kapp, P., and Zandt, G., 2009, Cyclicity in Cordilleran orogenic systems: Nature Geosciences, v. 2, p. 251–257.

DePaolo, D.J., 1981, A neodymium and strontium isotopic study of the Mesozoic calc-alkaline granitic batholiths of the Sierra Nevada and Peninsular Ranges, California: Journal of Geophysical Research, v. 86, p. 10,470–10,488.

Ducea, M., 2001, The California arc: Thick granitic batholiths, eclogite residues, lithospheric-scale thrusting, and magmatic flare-ups: GSA Today, v. 11, no. 11, p. 4–10.

Ducea, M., and Barton, M.D., 2007, Igniting flare-up events in Cordilleran arcs: Geology, v. 35, no. 1, p. 1047–1050.

Ducea, M.N., Kayzar, T., and Wetmore, P.H., 2009, High precision strontium isotopic analyses using multicollector ICP-MS, *in* Anastasiu, N., ed., Mineralogy and Geodiversity: Romanian Academy of Sciences Special Volume (in press).

Dufek, J., and Bergantz, G.W., 2005, Lower crustal magma genesis and preservation: A stochastic framework for evaluation of basalt–crust interaction: Journal of Petrology, v. 46, p. 2167–2195, doi: 10.1093/petrology/egi049.

Evenchick, C.A., 1991a, Geometry, evolution, and tectonic framework of the Skeena fold belt, north central British Columbia: Tectonics, v. 10, p. 524–546.

Evenchick, C.A., 1991b, Structural relationships of the Skeena fold belt west of Bowser Basin, Northwest British Columbia: Canadian Journal of Earth Sciences, v. 28, p. 973–983.

Evenchick, C.A., 2001, Northeast-trending folds in the western Skeena Fold Belt, northern Canadian Cordillera: A record of Early Cretaceous sinistral plate convergence: Journal of Structural Geology, v. 23, p. 1123–1140.

Friedman, R.M., Mahoney, J.B., and Cui, Y., 1995, Magmatic evolution of the southern Coast Belt: constraints from Nd–Sr isotopic systematics and geochronology of the southern Coast Plutonic Complex: Canadian Journal of Earth Sciences, v. 32, p. 1681–1698.

Galer, S.J.G., and Abouchami, W., 2004, Mass bias correction laws suitable for MC-ICPMS measurement: Geochimica et. Cosmochimica Acta, v. 68, A542–A542.

Gareau, S.A., and Woodsworth, G.H., 2000, Yukon-Tanana terrane in the Scotia-Quaal belt, Coast Plutonic Complex, central-western British Columbia, *in* Stowell, H.H., and McClelland, W.C., eds., Tectonics of the Coast Mountains, southeastern Alaska and British Columbia: Boulder, CO, Geological Society of America, p. 23–44.

Gehrels, G.E., and Boghossian, N.D., 2000, Reconnaissance geology and U–Pb geochronology of the west flank of the Coast Mountains between Bella Coola and Prince Rupert, costal British Columbia, *in* Stowell, H.H., and McClelland, W.C., eds., Tectonics of the Coast Mountains, southeastern Alaska and British Columbia: Boulder, CO, Geological Society of America, p. 61–75.

Gehrels, G.E., and Saleeby, J.B., 1987, Geologic framework, tectonic evolution, and displacement history of the Alexander terrane: Tectonics, v. 6, p. 151–173.

Gehrels, G.E., and Taylor, H.P., 1984, Fossil hydrothermal systems int he Ketchikan area, southeastern Alaska, *in* Coonrad, W.L., and Elliot, R.L., eds., The USGS in Alaska: Accomplishments during 1981: US Geological Survey, p. 134–137.

Gehrels, G.E., McClelland, W.C., Samson, S.D., Patchett, P.J., and Orchard, M.J., 1992, Geology of the western flank of the Coast Mountains between Cape Fanshaw and Taku Inlet, southeastern Alaska: Tectonics, v. 11, p. 567–585.

Gehrels, G.E., Rusmore, M., Woodsworth, G., Crawford, M., Andronicos, C., Hollister, L., Patchett, J., Ducea, M., Butler, R., Klepeis, K., Davidson, C., Mahoney, B., Friedman, R., Haggart, J., Crawford, W., and Pearson, J., In press, U–Th–Pb geochronology of the Coast Mountains Batholith in north-central British Columbia: Constrains on age, petrogenesis, and tectonic evolution: Geological Society of America Bulletin.

Gill, J.B., 1981, Orogenic andesites and plate tectonics: Berlin, Heidelberg, New York: Springer.

Girardi, J., Patchett, P.J., Ducea, M.N., Gehrels, G.E., Rusmore, M.E., Woodsworth, G.J., Pearson, D.M., and Manthei, C., 2009, Elemental and isotopic evidence for positive and negative feedback mechanisms governing, magmatic flux in the Coast Mountain Batholith, British Columbia: Earth and Planetary Science Letters (in review).

Goss, A.R., and Kay, S.M., 2006, Steep REE patterns and enriched Pb isotopes in southern Central American arc magmas: Evidence for forearc subduction erosions?: Geochemistry, Geophysics, and Geosystems, v. 7, no. Q05016, doi: 10.1029/2005GC001163.

Grove, T.L., Elkins-Tanton, L.T., Parman, S.W., Chatterjee, N., Muntener, O., and Gaetani, G.A., 2003, Fractional crystallization and mantle-melting controls on calc-alkine differentiation trends: Contributions to Mineralogy and Petrology, v. 145, p. 515–533.

Haggart, J.W., Diakow, L.J., Mahoney, J.B., Struik, L.C., Woodsworth, G.J., and Gordee, S.M., 2004, GeologyBella Coola area, British Columbia; Geological Survey of Canada, Open File 4639; British Columbia Geological Survey and Development Branch, Open Filer 2004-13, scale 1:50,000.

Harmon, R., and Hoefs, J., 1995, Oxygen isotope heterogeneity of the mantle deduced from global 18O systematics of basalts from different geotectonic settings: Contributions to Mineralogy and Petrology, v. 120, p. 95–114.

Hildreth, W., and Moorbath, S., 1988, Crustal contributions to arc magmatism in the Andes of central Chile: Contributions to Mineralogy and Petrology, v. 98, p. 455–489.

Hollister, L.S., and Andronicos, C.L., 2000, The Central Gneiss Complex, Coast Mountains, British Columbia, *in* Stowell, H.H., and McClelland, W.C., eds., Tectonics of the Coast Mountains, southeastern Alaska and British Columbia: Boulder, CO, Geological Society of America, p. 45–59.

Hollister, L.S., and Andronicos, C.L., 2006, Formation of new continental crust in western British Columbia during transpression and transtension: Earth and Planetary Science Letters, v. 249, p. 29–38.

Hutchison, W.W., 1982, 116 pp Geology of the Prince Rupert-Skeena map area, British Columbia: Memoir of the Geological Survey of Canada, v. 294.

Ingram, G.M., and Hutton, D.H.W., 1994, The Great Tonalite Sill: Emplacement into a contractional shear zone and implications for Late Cretaceous to early Eocene tectonics in southeastern Alaska and British Columbia: Geological Society of America Bulletin, v. 106, p. 715–728.

Jenner, G.A., Longerich, H.P., Jackson, S.E., and Fryer, B.J., 1990, ICP-MS – A powerful tool for high-precision trace-element analysis in Earth sciences: Evidence from analysis of selected U.S.G.S. reference samples: Chemical Geology, v. 83, nos. 1–2, p. 133–148.

Journeay, J.M., and Friedman, R.M., 1993, The Coast Belt thrust system: Evidence of Late Cretaceous shortening in southwest British Columbia: Tectonics, v. 12, p. 756–773.

Kistler, R.W., 1990, Two different lithospheric types in the Sierra Nevada, California, *in* Anderson, J.L., ed., The nature and origin of Cordilleran magmatism: Denver, CO: Geological Society of America, p. 271–281.

Kistler, R.W., and Peterman, Z.E., 1978, Variations in Sr, Rb, K, Na, and initial $^{87}Sr/^{86}Sr$ in Mesozoic granitic rocks and intruded wall rocks in central California: Geological Society of America Bulletin, v. 84, p. 3489–3512.

Klepeis, K.A., Crawford, M.L., and Gehrels, G.E., 1998, Structural history of the crustal-scale Coast shear zone north of Porland Canal, southeast Alaska and British Columbia: Journal of Structural Geology, v. 20, no. 7, p. 883–904.

Lassiter, J.C., DePaolo, D.J., and Mahoney, J.J., 1995, Geochemistry of the Wrangellia Flood Basalt Province: Implications for the role of continental and oceanic lithosphere in flood basalt genesis: Journal of Petrology, v. 36, p. 983–1005.

Longerich, H.P., Jenner, G.A., Fryer, B.J., and Jackson, S.E., 1990, Inductively coupled plasma-mass spectrometric analysis of geological samples: A critical evaluation based on case studies: Chemical Geology, v. 83, nos. 1–2, p. 105–118.

Magaritz, M., and Taylor, H.P., 1976, $^{18}O/^{16}O$ and D/H studies along a 500 km traverse across the Coast Ranges batholith and its country rocks, central British Columbia: Canadian Journal of Earth Sciences, v. 13, p. 1514–1536.

Magaritz, M., and Taylor, H.P., 1986, $^{18}O/^{16}O$ D/H studies of plutonic granite and metamorphic rocks across the Cordilleran batholiths of southern British Columbia: Journal of Geophysical Research, v. 91, p. 2193–2217.

Mahoney, J.B., Gordee, S.M., Haggart, J.W., Friedman, R.M., Diakow, L.J., and Woodsworth, G.J., In press, Magmatic evolution of the eastern Coast Plutonic Complex, Bella Coola Region, west central British Columbia: Geological Society of America Bulletin.

Mattey, D., Lowry, D., and Macpherson, C., 1994, Oxygen isotope composition of mantle peridotite: Earth and Planetary Science Letters, v. 128, p. 231–241.

McClelland, W.C., Gehrels, G.E., Samson, S.D., and Patchett, P.J., 1992, Structural and geochronologic relations along the western flank of the Coast Mountains batholith: Stinkine River to Cape Fanshaw, central SE Alaska: Journal of Structural Geology, v. 14, p. 475–489.

Monger, J.W., van der Hayden, P., Journeay, J.M., Evenchick, C.A., and Mahoney, J.B., 1994, Jurassic–Cretaceous basins along the Canadian Coast Belt: Their bearing on pre-mid-Cretaceous sinistral displacement: Geology, v. 22, p. 175–178.

Monger, J.W.H., Price, R.A., and Templeman-Kluit, D.J., 1982, Tectonic accretion and the origin of the two major metamorphic and plutonic welts in the Canadian Cordillera: Geololgy, v. 10, p. 70–75.

Pearce, J.A., 1983, Role of the sub-continental lithosphere in magma genesis at active continental margins, *in* Hawkesworth, C.J., and Norry, M.J., eds., Continental basalts and mantle xenoliths: Cheshire, UK: Shiva Publishing Ltd., p. 230–249.

Petford, N., and Atherton, M.P., 1996, Na-rich partial melts from newly underplated basaltic crust: the Cordillera Blanca batholith, Peru: Journal of Petrology, v. 37, no. 6, p. 1491–1521.

Rudnick, R.L., 1995, Making continental crust: Nature, v. 378, no. 6557, p. 571–578.

Rusmore, M.E., Gehrels, G.E., and Woodsworth, G.J., 2001, Southern continuation of the Coast Shear zone and Paleocene strain partitioning in British Columbia-southeast Alaska: Geological Society of America Bulletin, v. 113, p. 961–975.

Rusmore, M.E., Woodsworth, G.H., and Gehrels, G.E., 2000, Late Cretaceous evolution of the eastern Coast Mountains, Bella Coola, British Columbia, *in* Stowell, H.H., and McClelland, W.C., eds., Tectonics of the Coast Mountains, southeastern Alaska and British Columbia: Boulder, CO: Geological Society of America, p. 89–105.

Rusmore, M.E., Woodsworth, G.J., and Gehrels, G.E., 2005, Two-stage exhumation of mid-crustal arc rocks, Coast Mountains, British Columbia: Tectonics, v. 24, no. 5013, doi: 10.1029/204TC001750.

Samson, S.D., and Patchett, P.J., 1991, The Canadian Cordillera as a modern analog of Proterozoic crustal growth: Australian Journal of Earth Sciences, v. 38, no. 5, p. 595–611.

Samson, S.D., McClelland, W.C., Patchett, P.J., Gehrels, G.E., and Anderson, R.G., 1989, Evidence from neodymium isotopes for mantle contributions to Phanerozoic crustal genesis in the Canadian Cordillera: Nature, v. 337, no. 6209, p. 705–709.

Samson, S.D., Patchett, P.J., Gehrels, G.E., and Anderson, R.G., 1990, Nd and Sr isotopic characterization of the Wrangellia terrane and implications for crustal growth of the Canadian Cordillera: Journal of Geology, v. 98, p. 749–762.

Samson, S.D., Patchett, P.J., McClelland, W.C., and Gehrels, G.E., 1991a, Nd and Sr isotopic constraints on the petrogenesis of the west side of the northern Coast Mountains Batholith, Alaskan and Canadian Cordillera: Canadian Journal of Earth Sciences, v. 28, no. 6, p. 939–946.

Samson, S.D., Patchett, P.J., McClelland, W.C., and Gehrels, G.E., 1991b, Nd Isotopic characterization of metamorphic rocks in the Coast Mountains, Alaskan and Canadian Cordillera – Ancient crust bounded by juvenile terranes: Tectonics, v. 10, no. 4, p. 770–780.

Smith, T.E., Riddle, C., and Jackson, T.A., 1979, Chemical Variation within the Coast Plutonic Complex of British-Columbia between Lat 53-Degrees-N and 55-Degrees-N: Geological Society of America Bulletin, v. 90, no. 4, p. 346–356.

Stowell, H.H., and Crawford, M.L., 2000, Metamorphic history of the Coast Mountains orogen, western British Columbia and southeastern Alaska, *in* Stowell, H.H., and Crawford, M.L., eds., Tectonics in the Coastal Mountains, southeastern Alaska and British Columbia: Boulder, CO: Geological Society of America, p. 257–283.

Taylor, H.P., 1986, Igneous rocks: II. Isotopic case studies of circum-Pacific magmatism, *in* Valley, J.W., Taylor, H.P., and O'Neil, J.R., eds., Stable isotopes in high temperature geological processes: American Mineralogical Society, p. 273–318.

Taylor, H.P., and Sheppard, S.M.P., 1986, Igneous rocks: I. Processes of isotopic fractionation and isotope systematics, *in* Valley, J.W., Taylor, H.P., and O'Neil, J.R., eds., Stable isotopes in high temperature geological processes: American Mineralogical Society, p. 227–271.

Thibodeau, A.M., Killick, D.J., Ruiz, J., Chesley, J.T., Deagan, K., Cruxent, J.M., and Lyman, W., 2007, The strange case of the earliest silver extraction by European colonists in the New World: Proceedings of the National Academy of Sciences of the United States of America, v. 104, p. 3663–3666.

Thomas, J.B., and Sinha, A.K., 1999, Field, geochemical, and istopic evidence fro magma mixing and assimilation and fractionation crystallization processes in the Quottoon Igneous Complex, northwestern British Columbia and southeastern Alaska: Canadian Journal of Earth Sciences, v. 36, p. 819–831.

van der Heyden, P., 1992, A Middle Jurassic to Early Tertiary Andea-Sierran arc model for the Coast Belt of British Columbia: Tectonics, v. 11, p. 82–97.

Vervoort, J.D., Wirth, K., Kennedy, B., Sandland, T., and Harpp, K.S., 2007, The magmatic evolution of the Midcontinent Rift; new geochronologic and geochemical evidence from felsic magmatism: Precambrian Research, v. 157, p. 235–268.

Wheeler, J.O., and McFeely, P., 1991. Tectonic assemblage map of the Canadian Cordillera: Geological Survey of Canada Map 1712A.

Zartman, R.E., and Doe, B.R., 1981, Plumbotectonics-the model: Tectonophysics, v. 75, p. 135–162.

Zen, E., and Hammarstrom, J.M., 1984, Magmatic epidote and its petrologic significance: Geology, v. 12, p. 515–518.